metals

MDPI

Review

Review on the Research and Development of Ti-Based Bulk Metallic Glasses

Pan Gong [1], Lei Deng [1], Junsong Jin [1], Sibo Wang [1], Xinyun Wang [1,*] and Kefu Yao [2]

[1] State Key Laboratory of Materials Processing and Die & Mould Technology, Huazhong University of Science and Technology, Wuhan 430074, China; pangong@hust.edu.cn (P.G.); denglei@hust.edu.cn (L.D.); jsjin@hust.edu.cn (J.J.); M201670742@hust.edu.cn (S.W.)

[2] School of Materials Science and Engineering, Tsinghua University, Beijing 100084, China; kfyao@tsinghua.edu.cn

* Correspondence: bigaxun@263.net or wangxy_hust@hust.edu.cn; Tel./Fax: +86-27-8754-3491

Academic Editor: Jordi Sort Viñas

Received: 7 July 2016; Accepted: 18 October 2016; Published: 4 November 2016

Abstract: Ti-based bulk metallic glasses (BMGs) are very attractive for applications because of their excellent properties such as high specific strength and high corrosion resistance. In this paper, we briefly review the current status of the research and development of Ti-based bulk metallic glasses. Emphasis is laid on glass-forming ability, mechanical properties, corrosion resistance, and biocompatibility.

Keywords: Ti-based metallic glasses; glass-forming ability; mechanical properties; corrosion properties; biocompatibility

1. Introduction

Metallic glasses are alloys which possess disordered atomic-scale structure and contain short- to medium-range ordered clusters. In 1960, the first metallic glass was fabricated by rapid quenching a metallic liquid of $Au_{75}Si_{25}$ with a high cooling rate of 10^6 K/s [1]. In the 1970s and 1980s, metallic glasses could be directly made in bulk form by solidifying the melt at relatively low cooling rates (typically 10^3 K/s or less), where "bulk" is defined as that the minimum dimension of the alloy sample exceeds 1 mm. In 1974, the first reported bulk metallic glass (BMG) was developed in the Pd–Cu–Si alloy system by Chen et al. and only ϕ1–2 mm glassy samples could be prepared [2]. Then, extensive work was performed in exploring novel BMGs with good glass-forming ability (GFA). For instance, Inoue's group developed many classic glass-forming alloy systems, e.g., Pd–Cu–Ni–P [3,4], Zr–Cu–Ni–Al [5], La–Al–Cu–Ni [6], and Mg–Cu–Y [7]. Recently, the world's largest BMG with a diameter of 80 mm and a length of 85 mm was successfully prepared based on the $Pd_{42.5}Cu_{30}Ni_{7.5}P_{20}$ alloy [8]. Johnson's group developed a good glass former $Zr_{41.2}Ti_{13.8}Cu_{12.5}Ni_{10}Be_{22.5}$ (vit1) with a low critical cooling rate of ~1 K/s, which is the first commercial BMG and has been widely studied [9]. BMGs have been discovered in many alloy systems, such as Pd-based [10], Zr-based [11–13], Cu-based [14–16], Mg-based [17,18], Fe-based [19,20], Ni-based [21,22], Co-based [23,24], real earth-based [25,26], Pt-based [27], and Au-based [28] systems.

Among the metallic elements in the periodic table, titanium possesses ultrahigh specific strength together with high corrosion resistance and good biocompatibility. Accordingly, titanium alloys are widely used for structural, functional, and biomedical applications. Compared with conventional crystalline titanium alloys, Ti-based BMGs show higher specific strength and other unique properties because of the amorphous structure and are more attractive for practical applications as structural and functional materials [29,30]. In recent decades, Ti-based BMGs have received significant attention, and a large number of Ti-based BMGs have been developed. In this review, we summarize the details of the developments on the glass-forming ability, mechanical properties, corrosion resistance, and biocompatibility of Ti-based BMGs.

2. Glass-Forming Ability of Ti-Based BMGs

The formation of the first Ti-based amorphous alloys was reported in 1977 in Ti–Be–Zr ternary systems by Tanner [31]. Since then, several Ti-based glass-forming systems, such as Ti–Si [32], Ti–Ni [33], Ti–Be [34], Ti–Nb–Si [35], Ti–Al–Ni [36], and Ti–Zr–Cu [37], have been developed subsequently. However, the glass-forming ability (GFA) of these alloys is too low to form bulk metallic glass. In 1994, Peker et al. [38] reported Ti–Zr–Be–Ni alloys with wide supercooled liquid regions up to 45 K. As the large supercooled liquid region always entails a high thermal stability of the supercooled liquid against crystallization, these Ti–Zr–Be–Ni alloys were inferred to be potential bulk glass formers. In 1998, the first Ti-based BMG was successfully prepared by a copper mold casting in a Ti–Cu–Ni–Sn alloy system [39]. Encouraged by this success, with the effort of scholars all over the world, a number of Ti-based BMGs, such as Ti–Cu–Ni [40,41], Ti–Zr–Be [42,43], Ti–Zr–Cu–Ni–Sn [44,45], Ti–Zr–Cu–Pd–(Sn, Si, Nb) [46–50], Ti–Zr–Cu–Ni–Be [51–53], Ti–Zr–Hf–Cu–Ni–Si–Sn [54], and Ti–Cu–Zr–Fe–Sn–Si–(Ag, Sc) [55–57], have been developed over the last few decades. Figure 1 shows the maximum diameters for glass formation obtained in different alloy systems and the year in which they were discovered [8,58–73]. Compared with other alloy systems (e.g., Zr-, Pd-, Mg-, Fe-, Co-, Ni-, and Cu-based So far, the largest known critical diameter for Ti-based BMGs has been over 50 mm in the Ti–Zr–Cu–Ni–Be [72] and Ti–Zr–Cu–Fe–Be [73] quinary alloy systems. Only Pd- and Zr-based BMGs possess higher GFA. Figure 2 shows the X-ray diffraction (XRD) patterns and appearances of the developed $(Ti_{36.1}Zr_{33.2}Ni_{5.8}Be_{24.9})_{91}Cu_9$ and $Ti_{32.8}Zr_{30.2}Cu_9Fe_{5.3}Be_{22.7}$ fully glassy rods with critical diameters up to 50 mm [72,73].

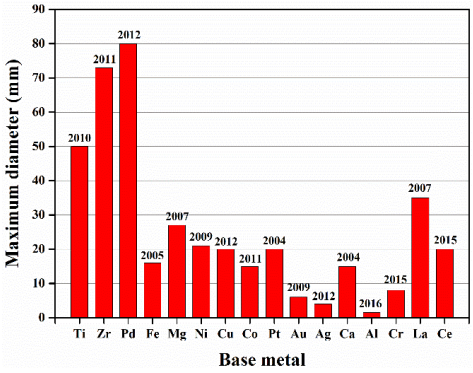

Figure 1. Maximum diameters of the bulk metallic glass (BMG) rods achieved in different alloy systems and the years in which they were discovered. Data are taken from [8,58–73].

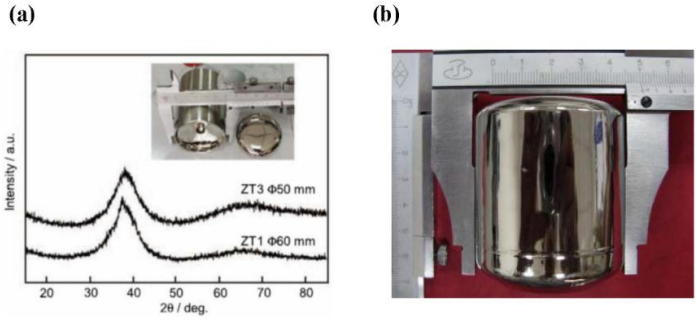

Figure 2. (**a**) X-ray diffraction (XRD) patterns of water-quenched $(Ti_{36.1}Zr_{33.2}Ni_{5.8}Be_{24.9})_{91}Cu_9$ rods with different diameters (inset is the picture of the 50 mm-diameter rod sample and 100 g pancake). Reproduced with permission from [72]. Copyright 2010, Elsevier. (**b**) The appearance of the 50 mm-diameter $Ti_{32.8}Zr_{30.2}Cu_9Fe_{5.3}Be_{22.7}$ rod sample prepared by copper mold casting. Reproduced with permission from [73]. Copyright 2015, Elsevier.

The GFA of BMGs can be directly evaluated by the critical cooling rate for glass formation, which is difficult to measure accurately. The critical diameter for glass formation (t_{max}) is a more practical measure of GFA, which has been widely used to compare the GFA of different BMGs but strongly depends on the fabrication condition. Hence, many quantitative criteria based on the thermal properties that can be easily measured by differential scanning calorimetry (DSC) have also been proposed to evaluate the GFA of BMGs [74–78]. The following three parameters are the most widely used: the width of the supercooled liquid region ΔT_x ($\Delta T_x = T_x - T_g$) [74], the reduced glass temperature T_{rg} ($T_{rg} = T_g/T_l$, sometimes use T_m instead of T_l) [75], and the γ parameter ($\gamma = T_x/(T_g + T_l)$) [76]. Here, T_g, T_x, T_m, and T_l are the glass transition temperature, the onset crystallization temperature, the melting temperature, and the liquidus temperature, respectively. Table 1 presents the details of the composition, the synthesis method, and the thermal properties of representative Ti-based BMGs that have been developed recently [39–41,45,47,49,52,55–57,73,79–110]. Copper mold casting is found to be the most frequently used method to prepare Ti-based BMGs. Compared with ΔT_x, the parameters T_{rg} and γ correlate better with t_{max} of Ti-based BMGs. All the Ti-based BMGs can be classified into three groups: Be- and Pd-free, Pd-containing, and Be-containing alloys. Based on the results summarized in Table 1, it has been found that although great progress has been achieved in the GFA of Ti-based BMGs, some technological drawbacks still exist. First, the titanium content of most developed Ti-based BMGs with high glass-forming ability is relatively low (<50 atom %). The addition of heavy elements (e.g., Pd, Cu, and Ni) improves the GFA but also increases the density. Second, all the developed centimeter-sized Ti-based BMGs contain toxic elements (e.g., Be) or noble elements (e.g., Pd). The largest critical diameter of Be- and Pd-free Ti-BMGs is only 7 mm [56]. Developing low cost and nontoxic Ti-based BMGs with high GFA is still very challenging.

Table 1. Thermal properties of typical Ti-based BMGs [39–41,45,47,49,52,55–57,73,79–110].

Composition (Atom %)	Synthesis Method	t_{max} (mm)	T_g (K)	T_x (K)	T_m (K)	T_l (K)	ΔT_x (K)	T_{rg}	γ	Heating Rate (K/min)	Ref.
$Ti_{50}Cu_{43}Ni_7$	Cu mold casting	1.5	667	704			37			40	[41]
$Ti_{53}Cu_{39}Ni_8$	Cu mold casting	1.5	658	698	1197	1219	40	0.539	0.372	40	[41]
$Ti_{55}Cu_{36}Ni_9$	Cu mold casting	1	652	692	1198	1221	40	0.582	0.369	40	[41]
$Ti_{50}Cu_{42}Ni_8$	Cu mold casting	2	657	713	1114	1168	56	0.563	0.391	40	[40]
$Ti_{40}Zr_{25}Be_{35}$	Cu mold casting	6	598	675		1125	76	0.532	0.392	20	[79]
$Ti_{45}Zr_{20}Be_{35}$	Cu mold casting	6	597	654		1123	57	0.531	0.380	20	[79]
$Ti_{41}Zr_{25}Be_{34}$	Cu mold casting	5	578	631			53			20	[80,81]
$Ti_{50}Zr_5Cu_{45}$	Cu mold casting	1									[82,83]
$Ti_{40}Zr_{10}Cu_{50}$	Cu mold casting	3	670	691	1121	1199	21	0.56	0.370	20	[82,83]
$Ti_{50}Ni_{20}Cu_{25}Sn_5$	Cu mold casting		710	770	1229		60			40	[39]
$Ti_{50}Ni_{15}Cu_{32}Sn_3$	Cu mold casting	1	686	759	1205	1283	73	0.53	0.385	20	[84]
$Ti_{38}Ni_{16.2}Cu_{37.8}Sn_8$	Cu mold casting	1	717	774			57			20	[85]
$Ti_{50}Zr_5Cu_{40}Ni_5$	Cu mold casting	2	634	685		1155	51	0.55	0.383	40	[82]
$Ti_{45}Zr_5Cu_{45}Ni_5$	Cu mold casting	3	673	715		1203	43	0.56	0.381	40	[82]
$Ti_{42.5}Zr_{10}Cu_{42.5}Ni_5$	Cu mold casting	3	651	695		1213	45	0.54	0.372	40	[82]
$Ti_{41.3}Cu_{43.7}Hf_{13.9}Si_{1.1}$	Cu mold casting	3	680	720			40			40	[82]
$Ti_{40}Zr_{10}Cu_{36}Pd_{14}$	Cu mold casting	6	669	718	1114	1191	49	0.56	0.386	40	[86]
$Ti_{40}Zr_{25}Be_{30}Cr_5$	Cu mold casting	8	599	692		1101	93	0.54	0.407	20	[79]
$Ti_{41}Zr_{25}Be_{28}Fe_6$	Cu mold casting	10	608	725		1143	117	0.53	0.414	20	[87]
$Ti_{40}Zr_{26}Be_{28}Fe_6$	Cu mold casting	10	615	715		1149	100	0.54	0.405	20	[88]
$(Ti_{41}Zr_{25}Be_{34})_{92}Fe_8$	Cu mold casting	10	619	730		1160	111	0.53	0.410	20	[89]
$Ti_{41}Zr_{25}Be_{28}Al_6$	Cu mold casting	7	624	691			67			20	[90]
$Ti_{41}Zr_{25}Be_{28}Ag_6$	Cu mold casting	10	597	655		1118	58	0.534	0.382	20	[91]
$Ti_{41}Zr_{25}Be_{28}Cu_6$	Cu mold casting	15	587	684		1130	97	0.520	0.398	20	[92]
$Ti_{41}Zr_{25}Be_{28}Ni_6$	Cu mold casting									20	[93]
$Ti_{50}Zr_{16}Be_{24}Ni_{10}$	Cu mold casting	5	605	661		1103	56	0.549	0.383	20	[94]
$Ti_{42.5}Zr_{7.5}Cu_{40}Ni_5Sn_5$	Cu mold casting	4	683	747		1217	64	0.561	0.393	20	[95]
$Ti_{43.15}Zr_{9.59}Cu_{36.24}Ni_{9.06}Sn_{1.96}$	Cu mold casting	3	649.5	699.5	986.8	1167.3	50	0.556	0.385	20	[45]
$Ti_{50}Cu_{20}Ni_{24}Si_4B_2$	Cu mold casting	1	735	800	1183	1214	65	0.605	0.410	40	[96]
$Ti_{48}Ni_{32}Cu_8Si_8Sn_4$	Cu mold casting	3	783.8	878.6			94.8			20	[97]
$Ti_{32.38}Cu_{42.34}Ni_{9.28}Zr_{7.6}Hf_{8.4}$	Cu mold casting	4	682	722	1111	1168	39	0.584	0.390	20	[98]
$Ti_{42.5}Zr_{2.5}Hf_5Cu_{42.5}Ni_{7.5}$	Cu mold casting	2	677	726	1143	1203	49	0.56	0.386	40	[99]
$Ti_{40}Zr_{10}Cu_{34}Pd_{14}Sn_2$	Cu mold casting	10	689	739	1126	1187	50	0.580	0.394	40	[47]
$Ti_{40}Zr_{10}Cu_{38}Pd_{10}Si_2$	Cu mold casting	5	685	750	1117	1193	65	0.574	0.399	40	[49]
$Ti_{32.8}Zr_{30.2}Ni_{5.3}Cu_9Be_{22.7}$	Water quenching	>50	611	655		961	44	0.636	0.417	20	[72]
$Ti_{40}Zr_{25}Ni_3Cu_{12}Be_{20}$	Cu mold casting	14	601	643		~985	42	0.610	0.405	20	[52]
$Ti_{40}Zr_{25}Ni_8Cu_9Be_{18}$	Cu mold casting	8	621	668	948	1009	47	0.63	0.410	40	[84]
$Ti_{32.8}Zr_{30.2}Cu_9Fe_{5.3}Be_{22.7}$	Cu mold casting	>50	578	658	946	1064	80	0.543	0.401	20	[73]

Table 1. *Cont.*

Composition (Atom %)	Synthesis Method	t_{max} (mm)	T_g (K)	T_x (K)	T_m (K)	T_l (K)	ΔT_x (K)	T_{rg}	γ	Heating Rate (K/min)	Ref.
$Ti_{36.2}Zr_{30.3}Cu_{8.3}Fe_4Be_{21.2}$	Cu mold casting	>30	576	638	928	1039	62	0.554	0.421	20	[100]
$(Ti_{41}Zr_{25}Be_{28}Fe_6)_{91}Cu_9$	Cu mold casting	>32	616	681	950	1108	65	0.556	0.395	20	[101]
$(Ti_{41}Zr_{25}Be_{29}Al_5)_{91}Cu_9$	Cu mold casting	10	637	705	938	1079	70	0.590	0.410	20	[102]
$Ti_{50}Ni_{15}Cu_{25}Sn_3Be_7$	Cu mold casting	2	688	741	1122	1207	45	0.57	0.387	40	[84]
$Ti_{50}Ni_{24}Cu_{20}B_1Si_2Sn_3$	Cu mold casting	1	726	800	1230	1310	74	0.59	0.393	40	[103]
$Ti_{45.8}Zr_{6.2}Cu_{39.9}Ni_{5.1}Sn_2Si_1$	Cu mold casting	4	670	711			35			20	[104]
$Ti_{41.5}Zr_{2.5}Hf_5Cu_{42.5}Ni_{7.5}Si_1$	Cu mold casting	5	680	730	1143	1199	50	0.57	0.389	40	[99]
$Ti_{47}Zr_{7.5}Cu_{40}Fe_{2.5}Sn_2Si_1$	Cu mold casting	3	646	702			56			20	[55]
$Ti_{45}Cu_{25}Ni_{15}Sn_3Be_7Zr_5$	Cu mold casting	5	685	741		1142	56	0.60	0.406	40	[105]
$(Ti_{40}Zr_{25}Be_{20}Cu_{12}Ni3)_{99.5}Y_{0.5}$	Cu mold casting	5	623	644	866	953	21	0.653	0.408	10	[106]
$Ti_{53}Cu_{15}Ni_{18.5}Al_7Sc_3Si_3B_{0.5}$	Cu mold casting	2	709	767		1240	58	0.619	0.394	40	[107]
$Ti_{53}Cu_{15}Ni_{18.5}Al_7Hf_3Si_3B_{0.5}$	Cu mold casting	2	695	749		1230	54	0.609	0.389	40	[107]
$Ti_{53}Cu_{15}Ni_{18.5}Al_7Zr_3Si_3B_{0.5}$	Cu mold casting	2.5	703	765		1237	62	0.57	0.394	40	[108]
$Ti_{53}Cu_{27}Ni_{12}Zr_3Al_7Si_3B_1$	Cu mold casting	2	685	754	1105		69			40	[109]
$Ti_{41.5}Zr_{2.5}Hf_5Cu_{37.5}Ni_{7.5}Si_1Sn_5$	Cu mold casting	6	693.33	752.52	1116.66	1176.07	64.19	0.590	0.405	20	[54]
$Ti_{46}Cu_{27.5}Zr_{11.5}Co_7Sn_3Si_1Ag_4$	Cu mold casting	5	640	691	1068	1207	51	0.530	0.374	20	[110]
$Ti_{47}Cu_{38}Zr_{7.5}Fe_{2.5}Sn_2Si_1Ag_2$	Cu mold casting	7	641	693	1116	1180	52	0.57	0.381	20	[56]
$Ti_{45}Cu_{40}Zr_{7.5}Fe_{2.5}Sn_2Si_1Sc_2$	Cu mold casting	6	637	692			55			20	[57]
$Ti_{44}Cu_{40}Zr_{7.5}Fe_{2.5}Sn_2Si_1Sc_3$	Cu mold casting	6	641	694			53			20	[57]

2.1. Alloy Development Studies

As most bulk metallic glasses are multicomponent alloys, the composition design of bulk metallic glasses has been acknowledged to be a difficult task. However, all the developed BMGs can be traced on the binary glassy alloys. According to the binary phase diagrams, Ti can form deep eutectics with Cu, Be, Pd, Si, Co, Ni, etc. By rapid cooling (e.g., sputtering or single roller spun-melt technique), amorphous thin films or ribbons were fabricated in these binary systems [32–34,111–113]. In order to improve the GFA of these binary alloys and obtain Ti-based BMGs, different alloying elements have been added to the binary alloys to explore multicomponent Ti-based bulk metallic glass-forming alloy systems. Except for the trial-and-error method, which is widely used but tedious and time-consuming, some empirical criteria have also been used for choosing the alloying elements. According to Inoue's classic three rules [114], the common characteristics of most bulk glass-forming alloy systems are (1) multicomponent systems consisting of more than three constituent elements; (2) significant differences in atomic sizes with a size ratio above 12% among the main constituent elements; and (3) negative heats of mixing among the main constituent elements. In this sense, the alloying elements should possess large atomic size mismatches and large values of negative heats of mixing against Ti. According to Table 1, we summarize the candidate constituent elements for developed Ti-based BMGs. Their atomic radii (R) and heats of mixing (ΔH_{mix}) against Ti are listed in Table 2 [115]. Generally, the classic empirical rules work well. There are also some special cases such as Sc, Y ($\Delta H_{Sc\text{-}Ti}$ = 8 kJ/mol, $\Delta H_{Y\text{-}Ti}$ = 15 kJ/mol), and Ag (R_{Ag} is similar as R_{Ti}). However, the content of these elements in Ti-based BMGs is relatively low. It has also been found that the substitution of similar atoms can markedly improve the glass-forming ability of BMGs [116]. Ti exhibits similar properties such as Zr, Hf, etc., while Cu can be replaced by similar atoms—Ni, Pd, or Ag. Therefore, based on the Ti–Cu binary system, multicomponent Ti(Zr, Hf)–Cu(Ni, Pd, Ag) alloys with higher GFA have been developed [82,86,98,99], indicating that this substitution method is also effective for exploring novel Ti-based BMGs.

Table 2. Atomic radii, Pauling electronegativity, and heats of mixing for some elements [115].

Element	Radiun (nm)	ΔH_{mix} (Ti) (kJ/mol)	R_{Ti}/R_A	$\|R_A - R_{Ti}\|/R_{Ti}$	Pauling Electronegativity
Ti	0.1462	—	1.000	0	1.54
Be	0.1128	−30	1.296	0.228	1.57
B	0.0820	−58	1.589	0.371	2.04
Al	0.1432	−30	1.021	0.021	1.61
Si	0.1153	−66	1.249	0.200	1.90
Sc	0.1641	8	0.891	0.122	1.36
V	0.1316	−2	1.111	0.100	1.63
Cr	0.1249	−7	1.171	0.146	1.66
Fe	0.1241	−17	1.178	0.151	1.83
Co	0.1251	−28	1.169	0.144	1.88
Ni	0.1246	−35	1.173	0.148	1.91
Cu	0.1278	−9	1.144	0.126	1.90
Y	0.1802	15	1.233	0.233	1.22
Zr	0.1603	0	0.913	0.096	1.33
Ag	0.1445	−2	1.012	0.012	1.93
Sn	0.1620	−21	0.925	0.081	1.96

As mentioned earlier, Ti-based BMGs can be classified into three groups: Be- and Pd-free, Pd-containing, and Be-containing alloys. In the rest of this section, typical alloy systems for each group are introduced in detail.

2.1.1. Be- and Pd-Free Ti-Based BMGs

This type of Ti-based BMG is mainly developed based on Ti–Cu binary systems [111]. The Ti–Cu–Ni alloy system, one of the typical representatives, is among the few Ti-based ternary systems with bulk glass-forming ability. In 2008, Wang et al. [41] investigated the GFA of the Ti–Cu–Ni ternary system systematically. Figure 3 shows the reported BMG-forming composition map of the Ti–Cu–Ni system. It can be seen that the BMG-forming composition region for t_{max} = 1 mm is located in the triangular region enclosed by the three intermetallic compounds TiNi, TiCu, and Ti_2Cu (50–57 atom % Ti, 34–44 atom % Cu, and 6–10 atom % Ni). The $Ti_{50}Cu_{43}Ni_7$ and $Ti_{53}Cu_{39}Ni_8$ alloys possess the best GFA, which enables the preparation of fully glassy rods with diameters up to 1.5 mm. It has also been found that the critical diameter increases to 2 mm by more fine-tuning of $Ti_{50}Cu_{43}Ni_7$ to $Ti_{50}Cu_{42}Ni_8$ [40]. Subsequently, it has been shown that the replacement of Ti by Zr effectively improves the GFA of Ti–Cu–Ni glassy alloys. By the "3D pinpoint approach," the BMG-forming maps for t_{max} = 1 mm was found in the composition range of 51–53 atom % (Ti + Zr), 38–41 atom % Cu, and 8–10 atom % Ni (as shown in Figure 4) [41]. This incentive played a trigger effect on the subsequent development of new Ti-based BMGs with critical diameters ranging from 1 to 6 mm, such as Ti–Zr–Cu [82,83], Ti–Zr–Cu–Ni [82], Ti–Zr–Cu–Ni–Sn [45,95], Ti–Zr–Cu–Ni–Sn–Si [104], Ti–Zr–Hf–Cu–Sn–Si [99], and Ti–Zr–Hf–Cu–Ni–Si–Sn [54]. Recently, a novel strategy for designing BMG with high mixing entropy and large GFA has been proposed. Using this method, a series of Ti–Cu–Zr–Fe(Co)–Sn–Si–Ag(Sc) [56,57] BMGs has been discovered by multi-substitution of similar elements. After multi-substitution, the mixing entropy of the alloys is significantly enhanced, and the crystallization process exhibits a higher level of complexity, implying a better GFA. It is worth mentioning that the critical diameter for glass formation was reported to be 7 mm for $Ti_{47}Cu_{38}Zr_{7.5}Fe_{2.5}Sn_2Si_1Ag_2$ alloy [56], which is the largest among the Be- and Pd-free Ti-based BMGs.

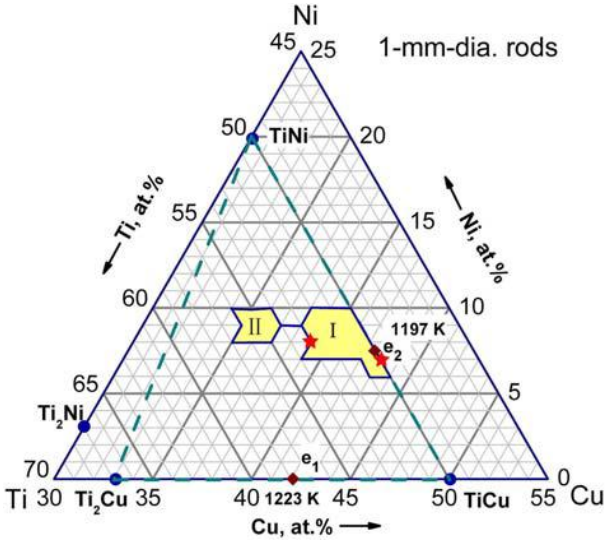

Figure 3. BMG formation composition zone with t_{max} = 1 mm in the ternary Ti–Cu–Ni system. Reproduced with permission from [41]. Copyright 2008, Springer.

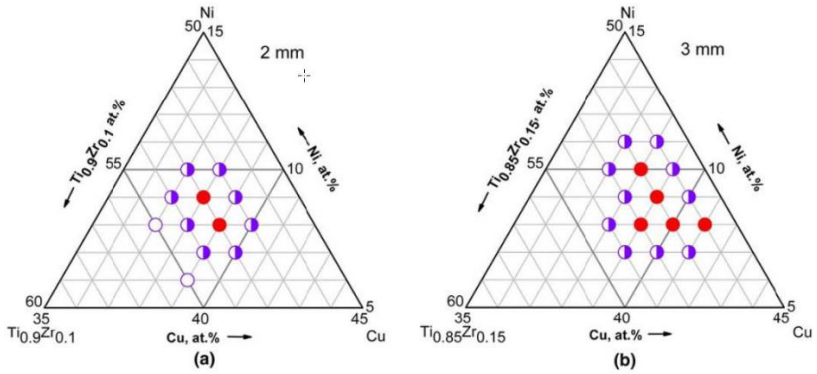

Figure 4. Composition maps of BMG formation in the $(Ti_{1-x}Zr_x)$–Cu–Ni system. The two panels, (a) and (b), show the BMG-forming composition ranges at two ratios of $Ti_{1-x}Zr_x$, (**a**) x = 0.1 and (**b**) x = 0.15, for the as-cast rods of 2 and 3 mm in diameter, respectively. Reproduced with permission from [41]. Copyright 2008, Springer.

2.1.2. Pd-Containing Ti-Based BMGs

This type of Ti-based BMG was firstly developed in the Ti–Zr–Cu–Pd system in 2007 [86]. Since Pd possesses properties similar to Cu, Pd was introduced to partially substitute for Cu to improve the GFA. It was noticed that a series of 6 mm-diameter Ti–Zr–Cu–Pd alloys were produced, and the largest critical diameter of Ti–Zr–Cu–Pd quaternary alloy was up to 7 mm. In order to further improve the GFA, Zhu et al. investigated the addition of Sn on the GFA of Ti–Zr–Cu–Pd BMG [47]. With the addition of 2–4 atom % Sn, the critical diameter was markedly increased to 10 mm, which is larger than that of other Be-free Ti-based BMGs. Figure 5 shows the appearance of the as-cast 10 mm-diameter $Ti_{40}Zr_{10}Cu_{34}Pd_{14}Sn_2$ and $Ti_{40}Zr_{10}Cu_{32}Pd_{14}Sn_4$ rods. Except Sn, Si [49], Nb [50] and Co [117] have also been adopted as alloying elements for Ti–Zr–Cu–Pd quaternary alloys. The maximum critical diameters of Ti–Zr–Cu–Pd–Si, Ti–Zr–Cu–Pd–Nb, and Ti–Zr–Cu–Pd–Co were reported to be 5 mm, >2 mm, and 10 mm, respectively. Without biological toxic elements such as Be, Ni, and Al, these Ti-based BMGs are expected to be used as biomedical materials. The limitation is that, because of the noble element Pd, the cost of this type of Ti-based BMG is relatively high.

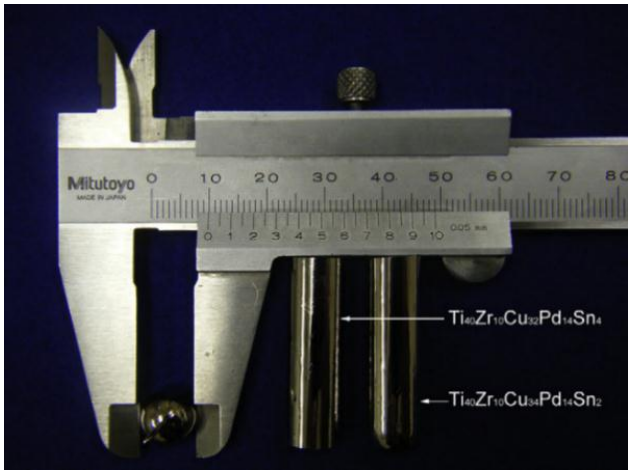

Figure 5. Outer surface of cast $Ti_{40}Zr_{10}Cu_{34}Pd_{34}Sn_2$ and $Ti_{40}Zr_{10}Cu_{32}Pd_{14}Sn_4$ BMG rods with a diameter of 10 mm. Reproduced with permission from [47]. Copyright 2008, Elsevier.

2.1.3. Be-Containing Ti-BMGs

This type of Ti-based BMG is mainly developed based on the Ti–Be binary system [34]. Be is a magic metallic element with unique properties. The density of Be is only 1.85 g/cm^3, which is much lower than that of Ti (4.50 g/cm^3). Therefore, Be–bearing Ti-based BMGs exhibit relatively low density and high specific strength compared with Be-free Ti-based BMGs. Moreover, as the atomic radius of Be is much smaller than that of most metallic atoms (as shown in Table 1), it has been found that the addition of Be significantly improves the GFA of Zr- [118,119], Cu- [120], and Ti-based BMGs [79–81]. Except for the Ti–Cu–Ni system mentioned in Section 2.1.1, the Ti–Zr–Be system is another important Ti-based ternary system with bulk glass-forming ability. In 2008, Duan et al. firstly reported a series of lightweight Ti–Zr–Be BMGs with critical diameters larger than 6 mm [79]. Without containing heavy late transition metals (e.g., Cu, Ni, and Fe), the density of these alloys was lower than 5 g/cm^3, resulting in a high specific strength larger than 400 J/g, which is more than twice that of the commercial Ti–6Al–4V (the most widely used crystalline titanium alloy). In 2010, Zhang et al. systematically studied the GFA of the Ti–Zr–Be system [80,81]. As shown in Figure 6, two amorphous regions were found in the Ti–Zr–Be system. The first amorphous region includes two intermetallic compounds (BeTi and Be_2Zr) and one solid solution (α-Ti). The second amorphous region contains only one intermetallic compound (Be_2Zr) and two solid solutions (α-Ti and β-Zr) and exhibits better GFA (t_{max} = 5 mm) compared with the first one (t_{max} = 3 mm). This may be because intermetallic compounds are easier to be suppressed as they are always ordered phases. Based on experimental results, the best glass former was located at $Ti_{41}Zr_{25}Be_{34}$, which is close to the predicted composition by binary-eutectic rule ($Ti_{41}Zr_{32}Be_{27}$). Then, a series of Ti–Zr–Be–(Fe, Al, Ag, Cu, Ni, V, Cr) BMGs [79–81,87–94] with improved GFA was reported, and some of the developed quaternary alloys were found to possess a larger critical size up to a centimeter scale. A pseudo Ti–Zr–Cu–Ni–Be system, which possesses a much higher GFA, was discovered based on the Ti–Zr–Be system. In 2005, Park et al. evaluated the GFA of Ti–Zr–Cu–Ni–Be alloys by injection copper mold casting and systematically outlined the alloy composition ranges with a t_{max} larger than 1, 6, and 10 mm, as shown in Figure 7 [121]. In 2010, a breakthrough was made in the GFA of Ti–Be-based BMGs by Tang et al [72]. They found that the microstructure of a $Ti_{50}Zr_{23}Ni_3Cu_6Be_{18}$ as-cast pancake mainly consisted of a primary β-Ti phase and an amorphous phase. Based on the composition of the amorphous phase, which promises higher GFA than that of $Ti_{50}Zr_{23}Ni_3Cu_6Be_{18}$, they prepared a high number of pancakes with compositions nearby and measured the compositions of the corresponding amorphous phases. Using this technique, a series of Ti–Zr–Ni–Be–Cu BMGs with high GFA have been developed. It was reported that $(Ti_{36.1}Zr_{33.2}Ni_{5.8}Be_{24.9})_{91}Cu_9$ is formable as a BMG alloy with a larger

diameter of 50 mm via water quenching, which is a new record in the GFA of Ti-based BMGs [72]. By replacing Ni with similar atom Fe, Ti–Zr–Cu–Fe–Be BMGs with critical diameters up to 50 mm have also been developed [73]. By direct solidification, a 150 g $Ti_{36.2}Zr_{30.3}Cu_{8.3}Fe_4Be_{21.2}$ amorphous ingot was successfully prepared, indicating a superior GFA. Ti–Be-based BMGs possess low density and high strength together with high GFA, which favors their application as high performance structural materials. However, their application is also constrained to an extent because of the toxicity of Be.

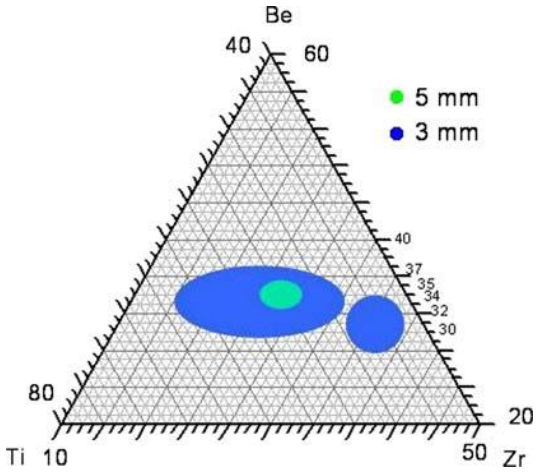

Figure 6. Glass-formation zones of 3 mm and 5 mm rods in the Ti–Zr–Be ternary alloy system. Reproduced with permission from [43]. Copyright 2010, Springer.

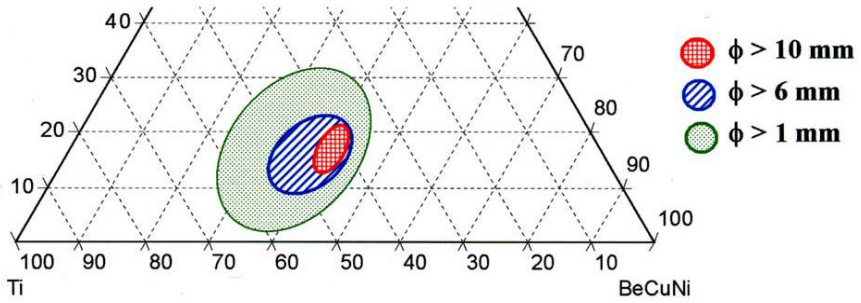

Figure 7. Schematic pseudo Ti–Zr–(Cu, Ni, Be) ternary diagram showing the outline of composition range for maximum diameter for glass formation of 1, 6, and 10 mm. Reproduced with permission from [121]. Copyright 2005, Elsevier.

2.2. Role of Alloying Elements on GFA

Alloying additions have been widely applied to develop new metallic crystalline materials and optimize the properties of these alloys. Recently, this technique was proved to be a simple but effective way to improve the GFA of BMGs [122–124]. In this section, we will focus on the effect of alloying on the GFA of Ti-based BMGs. Table 3 summarizes the effects of different alloying elements on the thermal stability (reflected by ΔT_x) and GFA of Ti-based BMGs [39,49,52,54,57,79,87,90–92,99,105–108,110,117,125–130].

Table 3. Summary of the effects of alloying elements on the glass-forming ability (GFA) of various Ti-based BMGs [39,49,52,54,57,79,87,90–92,99,105–108,110,117,125–130].

Alloying Element	Optimum Content x (Atom %)	Base Alloy (Atom %)	t_{max} (mm)			ΔT_x (K)			Ref.
			Without	With	Increment	Without	With	Extension	
B	0.2–0.8	$Ti_{53}Cu_{22-x}Ni_{12}Zr_3Al_7Si_3B_x$			Improved				[108]
N	0.1	$(Ti_{42.5}Cu_{40}Zr_{10}Ni_5Sn_{2.5})_{100-x}N_x$	3	4	1	46.7	44.1	−2.6	[125]
	1	$Ti_{46}Cu_{31.5}Zr_{12.5-x}Co_7Sn_3Si_x$	2	3	1				[126]
Si	1	$Ti_{42.5-x}Zr_{2.5}Hf_5Cu_{42.5}Ni_{7.5}Si_x$	2	5	3	49	50	1	[99]
	2	$Ti_{40}Zr_{10}Cu_{40-x}Pd_{10}Si_x$	4	5	1	50	65	15	[49]
Al	5	$Ti_{41}Zr_{25}Be_{34-x}Al_x$	5	7	2	57	70	13	[90]
Sc	2	$Ti_{47-x}Cu_{40}Zr_{7.5}Fe_{2.5}Sn_2Si_1Sc_x$	3	6	3	54	55	1	[57]
Cr	5	$Ti_{40}Zr_{25}Be_{35-x}Cr_x$	6	8	2	53	97	44	[79]
Fe	6	$Ti_{41}Zr_{25}Be_{34-x}Fe_x$	5	10	5	57	117	60	[87]
Co	1	$(Ti_{0.4}Zr_{0.1}Cu_{0.36}Pd_{0.14})_{100-x}Co_x$	5	8	3	49	59	10	[117]
Ni	3	$Ti_{40}Zr_{25}Cu_{15-x}Ni_xBe_{20}$	10–14	>14	Improved	48	42	−6	[52]
Cu	6	$Ti_{41}Zr_{25}Be_{34-x}Cu_x$	5	15	10	57	97	40	[92]
Y	0.5	$(Ti_{40}Zr_{25}Be_{20}Cu_{12}Ni_3)_{100-x}Y_x$	<5	5	Improved	42	21	−21	[106,127]
Zr	5	$Ti_{50-x}Cu_{25}Ni_{15}Sn_3Be_7Zr_x$	5	6	1	45	56	11	[105]
Nb	3	$(Ti_{40}Zr_{25}Cu_9Ni_8Be_{18})_{100-x}Nb_x$				40	46	6	[128,129]
Ag	4	$Ti_{46}Cu_{31.5-x}Zr_{11.5}Co_7Sn_3Si_1Ag_x$	3	5	2	51	51	0	[110]
	6	$Ti_{41}Zr_{25}Be_{34-x}Ag_x$	5	10	5	57	58	1	[91]
Sn	2	$(Ti_{0.45}Cu_{0.378}Zr_{0.10}Ni_{0.072})_{100-x}Sn_x$	1	2	1	39	42	3	[130]
	5	$Ti_{41.5}Zr_{2.5}Hf_5Cu_{42.5-x}Ni_{7.5}Si_1Sn_x$	2	6	4	35	64	29	[54]
Sb	3	$Ti_{50}Cu_{25}Ni_{25-x}Sb_x$				40	45	5	[39]
Hf	5	$Ti_{47.5-x}Zr_{2.5}Hf_xCu_{42.5}Ni_{7.5}$	1	2	1	47	49	2	[99]

2.2.1. The Additions of Metalloid Elements

Metalloid elements (such as O, N, B, and Si) have a strong affinity with Ti and can be absorbed during the preparation process of Ti-based BMGs. Therefore, it is necessary to investigate the effect of metalloid elements on the GFA of Ti-based BMGs. It was reported that a high oxygen concentration has a detrimental effect on glass formation for Zr-based BMGs [131,132]. As Ti possesses similar properties as Zr and easily reacts with oxygen, it can be inferred that oxygen introduced from the raw materials or the low vacuum may have a negative effect on GFA of Ti-based BMGs. Experimental results indicate that the GFA of $Ti_{42.5}Cu_{40}Zr_{10}Ni_5Sn_{2.5}$ is sensitive to the nitrogen doping level [125]; with the addition of less than 0.1 atom % nitrogen, the GFA is improved because of the suppression of the formation of a competing eutectic structure. However, if the nitrogen concentration exceeds 0.1 atom %, the formation of quasicrystals can be promoted, and the GFA is deteriorated. A minor Si addition also shows a great effect on the thermal stability and GFA of Ti-based BMGs. For example, a 2 atom % Si addition to Ti–Zr–Cu–Pd BMG can extend the ΔT_x from 50 K to 65 K, indicating an improvement in the thermal stability [49]. Substituting 1 atom % Ti with Si in a $Ti_{42.5}Zr_{2.5}Hf_5Cu_{42.5}Ni_{7.5}$ alloy increases the critical diameter from 2 mm to 5 mm [99]. Because of the relatively small atomic size, the minor amount of Si may facilitate the formation of a denser atomic structure and stabilize the supercooled liquid. However, as Si exhibits large negative heats of mixing against most constituent elements of Ti-based BMGs (e.g., $\Delta H_{Si-Ti} = -66$ kJ/mol), an excessive addition of Si is detrimental to the GFA due to the formation of intermetallic compounds.

2.2.2. The Additions of Metallic Elements

The intermediate metallic atoms such as Fe, Ni, Cu, Co, and Nb have been widely used as alloying elements in various alloy systems. It was reported that only when the alloying quantities exceed 5 atom % have they been shown to be beneficial in bulk glass formation [123]. For Ti-based BMGs, this argument is supported by some examples listed in Table 3. For example, in order to improve the GFA of a $Ti_{41}Zr_{25}Be_{34}$ alloy, the alloying quantities of Fe, Al, Cu, Ni, or Cr have to be over 5 atom % [79,87–92]. However, there are contrary examples. According to Guo et al.'s research [52], the optimum Ni content in the $Ti_{40}Zr_{25}Cu_{15-x}Ni_xBe_{20}$ system is no more than 3 atom %. Moreover, the GFA of Ti–Zr–Cu–Pd BMG can be markedly improved by the addition of only 1 atom % Co, and the critical diameter is increased from 3 mm to 5 mm [117].

The addition of large atoms (e.g., Zr, Sn, and Sc) has been proved to be beneficial in increasing the atomic size difference and improving the GFA of Ti-based BMGs. For instance, Sn is an effective alloying element to developing Pd- and Be-free Ti-based BMGs with high GFA. By replacing 5 atom % of Cu with Sn in a $Ti_{41.5}Zr_{2.5}Hf_5Cu_{42.5}Ni_{7.5}Si_1$ alloy, the supercooled liquid region can be extended by 29 K, and the critical diameter is also drastically enhanced from 2 mm to 6 mm [54]. Moreover, Sc has been found to be able to not only alleviate the harmful effect of oxygen impurity but also influence the formation of topological and chemical short-range orders. With the addition of 2 atom % Sc, the critical diameter of the $Ti_{47}Cu_{40}Zr_{7.5}Fe_{2.5}Sn_2Si_1$ alloy is increased from 3 mm to 6 mm [57].

Among all the metallic elements, Be possesses the smallest atomic size. As shown in Table 1, the Be-containing Ti-based BMGs possess higher GFA compared with Be-free Ti-based BMGs, indicating that the addition of Be is effective in enhancing the GFA of Ti-based BMGs. Moreover, the addition of Be also increases the specific strength of Ti-based BMGs. As Be is a toxic element, it is hoped that the GFA of Ti-based BMGs can be significantly enhanced with minimal Be content. However, the Be content in Ti-based BMGs is always over 5 atom %. Little work has been done on the effect of the minor addition of Be (<2 atom %) on the GFA of Ti-based BMG forming systems.

2.2.3. The Additions of Rare-Earth Elements

Rare-earth elements possess unique physical and chemical properties, so they have been widely used as minor additions for metallic materials. Yttrium is the most widely used real earth element

to tailor the properties of BMGs [133,134]. It was found that the addition of 0.5 atom % yttrium can effectively increase the GFA of $Ti_{40}Zr_{25}Be_{20}Cu_{12}Ni_3$ alloys and enables the formation of 5 mm-diameter glassy rods using low purity raw materials [106,127]. It is well known that oxygen is suspected to form titanium oxide at higher temperatures, which acts as crystallization nuclei. A small and proper amount of yttrium addition can scavenge oxygen from the supercooled liquid to suppress the precipitation of the Laves phase and lower the liquidus temperature. The large atomic size of yttrium also plays an important role in increasing the atomic packing efficiency and improving the GFA.

2.3. Prediction of GFA of Ti-Based BMGs

The search for novel BMGs is still mainly based on trial-and-error although a few empirical guides (e.g., Inoue's three rules) have been proposed. It is important to develop a simple and unified criterion that can characterize the GFA of BMGs. The GFA of BMGs is directly reflected by the critical cooling rate R_c and the critical diameter t_{max}. However, R_c measurement is complex, while t_{max} is affected by the preparation conditions. Therefore, researchers have established GFA parameters or criteria based on the characteristic temperatures (e.g., T_g, T_x, T_m, and T_l), which can be determined by DSC, such as ΔT_x, T_{rg}, and γ, mentioned at the beginning of this section. These parameters are good in practicability but cannot intrinsically reflect the origin of GFA.

The GFA is an inherent property and should relate to the intrinsic factors of BMGs. Thus, it is important to determine the key factors influencing the GFA. Much research shows that atomic size differences between the constituent elements and the heat of mixing play important roles on the glass formation of BMGs [135–137]. Recently, it has been found that the electronegativity difference also influences the GFA of Al- [138,139], Fe-[140], and Ti-based BMGs [90–93]. In order to evaluate the GFA of Ti-based BMGs, Zhao et al. [93] calculated the parameters including the atomic size difference δ, electronegativity difference Δx, and the enthalpy of mixing ΔH_{mix} for typical Ti-based BMGs. As shown in Figure 8, the high GFA of Ti-based BMGs ($t_{max} \geq 10$ mm) requires an optimal combination of atomic size difference δ, electronegativity difference Δx, and the enthalpy of mixing ΔH_{mix}: $0.1176 \leq \delta \leq 0.1333$, $0.1194 \leq \Delta x \leq 0.1837$, and -23.81 kJ/mol $\leq \Delta H_{mix} \leq -33.15$ kJ/mol. These rules provide new insight and valuable guidance for the future development of Ti-based BMGs with higher GFA.

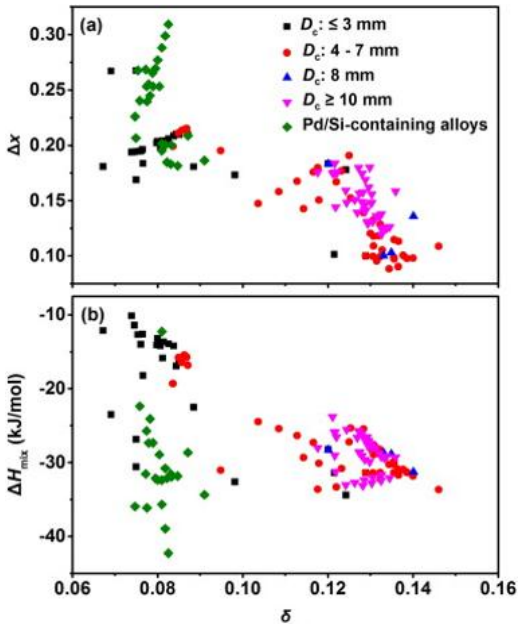

Figure 8. The distribution of Δx and ΔH_{mix} values of all the developed Ti-based BMGs with their atomic size difference δvalues. Reproduced with permission from [93]. Copyright 2015, Elsevier.

3. The Mechanical Properties of Ti-Based BMGs

Compared with crystalline Ti alloys, Ti-based BMGs exhibit outstanding mechanical properties such as large elastic limit, higher specific strength, and higher hardness [141–143]. Consequently, Ti-based BMGs can be exploited for structural applications. However, as other BMGs, Ti-based BMGs also have drawbacks that make their use for engineering applications appear challenging.

3.1. Elastic Properties

Figure 9 summarizes the relationship between the Young's modulus and tensile fracture strength of typical BMGs together with classic engineering materials [144]. Table 4 lists the Young's modulus and Poisson's ratio of typical Ti-based BMGs [40,41,45,47,49,52–57,72,79–82,84,86–95,99–106,110,126,145–147]. Compared with conventional Ti crystalline alloys, Ti-based BMGs possess a lower Young's modulus but higher fracture strength and larger elastic strain (close to 2.0%). The elastic strain energy of Ti-BMGs is larger than 20.0 MJ/m^2 (e.g., $Ti_{41.5}Zr_{2.5}Hf_5Cu_{42.5}Ni_{7.5}Si_1$ BMG), which is more than eight times that of the best spring steel [148]. There is also a correlation between the elastic properties (e.g., Young's modulus E and Poisson's ratio ν) and room temperature plasticity of BMGs. It was reported that BMGs with a higher Poisson's ratio (e.g., >0.32) may possess larger plasticity [149,150]. In this sense, Ti-based BMGs can be classified as "ductile" because of the relatively high Poisson's ratio.

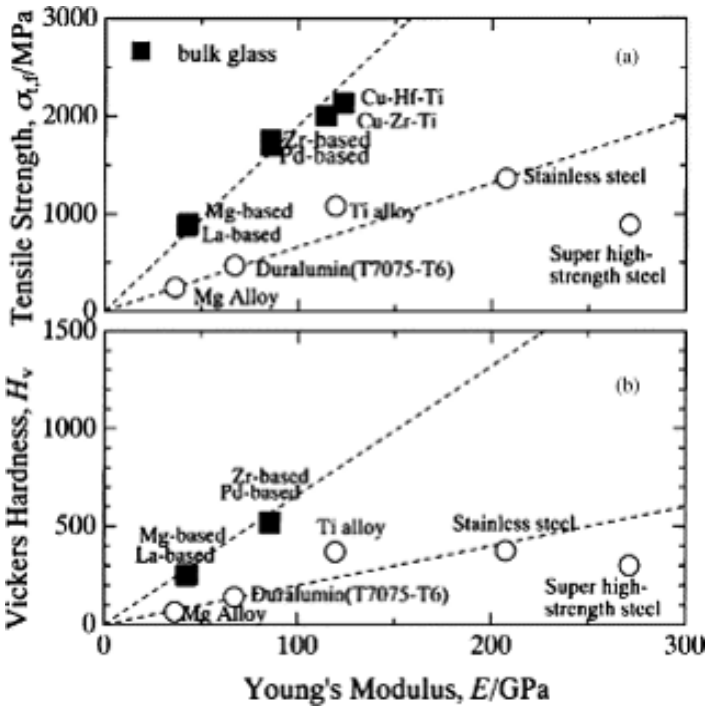

Figure 9. The relations between mechanical properties of typical BMGs: (**a**) tensile fracture strength $\sigma_{t,f}$ with Young's modulus E; (**b**) Vickers hardness H_v with Young's modulus E. Reproduced with permission from [144]. Copyright 2002, The Japan Institute of Metals and Materials.

Table 4. Mechanical properties of typical Ti-based BMGs together with other BMGs and crystalline alloys [40,41,45,47,49,52–57,72,79–82,84,86–95,99–106,110,126,145–147].

Composition (atom %)	Density (g/mm^3)	σ_y (MPa)	σ_{max} (MPa)	ε_p (%)	σ_c (N·m/kg)	Sample Size (mm)	Stain Rate (s^{-1})	*E* (GPa)	ν	Ref.
$Ti_{50}Cu_{43}Ni_7$			2050	5–11		ϕ1 × 2	1×10^{-4}			[41]
$Ti_{53}Cu_{39}Ni_8$			2160	0–6		ϕ1 × 2	1×10^{-4}			[41]
$Ti_{55}Cu_{36}Ni_9$										[41]
$Ti_{50}Cu_{42}Ni_8$			2008	0		ϕ2 × 4	3×10^{-4}	100		[40]
$Ti_{45}Zr_{20}Be_{35}$	4.59		1860	2.2	4.05×10^5	ϕ3 × 6	1×10^{-4}	96.8	0.36	[79]
$Ti_{41}Zr_{25}Be_{34}$	4.88	1891	2238	8.2	3.88×10^5	ϕ2 × 4	1×10^{-4}			[80,81,87]
$Ti_{45}Zr_5Cu_{45}Ni_5$			1926	1.8		ϕ2 × 4	4×10^{-4}	110		[82]
$Ti_{41.3}Cu_{43.7}Hf_{13.9}Si_{1.1}$			1685	0		ϕ3 × 6	5×10^{-4}	95		[145]
$Ti_{40}Zr_{10}Cu_{36}Pd_{14}$	~7.20		1950	0.5	2.7×10^5	ϕ2.5 × 5	5×10^{-4}	82		[86]
$Ti_{40}Zr_{25}Be_{30}Cr_5$	4.76	1720	1900	3.5	3.61×10^5	ϕ3 × 6	1×10^{-4}	94.8	0.35	[79]
$Ti_{41}Zr_{25}Be_{28}Fe_6$	4.88	1964	2268	112	4.02×10^5	ϕ2 × 4	4×10^{-4}			[87]
$Ti_{40}Zr_{26}Be_{28}Fe_6$	4.93	1989	2162	7.4	4.03×10^5	ϕ2 × 4	4×10^{-4}			[88]
$(Ti_{41}Zr_{25}Be_{28})_{94}Fe_6$	4.94	2018	2101	0.8	4.09×10^5	ϕ2 × 4	4×10^{-4}			[89]
$Ti_{41}Zr_{25}Be_{28}Al_6$	4.80	1996	2190	16.3	4.16×10^5	ϕ2 × 4	4×10^{-4}			[90]
$Ti_{41}Zr_{25}Be_{28}Ag_6$	5.27	1961	2013	2.3	3.73×10^5	ϕ2 × 4	4×10^{-4}			[91]
$Ti_{41}Zr_{25}Be_{28}Cu_6$	5.02	1869	1926	2.7	3.72×10^5	ϕ2 × 4	4×10^{-4}			[92]
$Ti_{41}Zr_{25}Be_{28}Ni_6$	5.07	1889	1933	4.8	3.73×10^5	ϕ2 × 4	4×10^{-4}			[93]
$Ti_{50}Zr_{16}Be_{24}Ni_{10}$	4.99	1900	2000	5.7	3.81×10^5	ϕ2 × 4	4×10^{-4}			[94]
$Ti_{65}Cu_9Ni_8Be_{18}$	4.84	2183	2250	0.7	4.51×10^5	ϕ2 × 4	1×10^{-4}	110	0.351	[53]
$Ti_{42.5}Zr_{7.5}Cu_{40}Ni_5Sn_5$		1978	2162	0.9		ϕ2.5 × 5	4×10^{-4}			[95]
$Ti_{43.15}Zr_{9.59}Cu_{36.24}Ni_{9.06}Sn_{1.96}$	6.60	2360	2640	2.24	3.58×10^5	ϕ1 × 2	4×10^{-4}	103		[45]
$Ti_{40}Zr_{10}Cu_{34}Pd_{14}Sn_2$	6.85	2000	2050	3.5	2.9×10^5	ϕ2 × 4	5×10^{-4}			[47]
$Ti_{40}Zr_{10}Cu_{38}Pd_{10}Si_2$			1935	0		ϕ2.5 × 5	5×10^{-4}	80		[49]
$Ti_{60}Zr_5Cu_9Ni_8Be_{18}$	4.98	2183	2250	0.7	4.3×10^5	ϕ2 × 4	1×10^{-4}	106	0.352	[53]
$Ti_{55}Zr_{10}Cu_9Ni_8Be_{18}$	5.03	2050	2113	8.3	4.1×10^5	ϕ2 × 4	1×10^{-4}	98	0.356	[53]
$Ti_{40}Zr_{25}Cu_{12}Ni_3Be_{20}$	5.38	1680	1780	5	3.1×10^5	ϕ3 × 6		92.6		[52]
$Ti_{32.8}Zr_{30.2}Ni_{5.3}Cu_9Be_{22.7}$	5.541		1831	0	3.30×10^5	ϕ2 × 4	1×10^{-4}	97.8	0.354	[72]
$(Ti_{41}Zr_{25}Be_{29}Al_5)_{91}Cu_9$	5.07	2093	2209	0.6	4.13×10^5	ϕ2 × 4	4×10^{-4}			[102]
$(Ti_{41}Zr_{25}Be_{28}Fe_6)_{91}Cu_9$	5.36	1999	2083	1.2	3.7×10^5	ϕ2 × 4	4×10^{-4}			[101]
$Ti_{36.2}Zr_{30.3}Cu_{8.3}Fe_4Be_{21.2}$		1680	1940	8		ϕ2 × 4	1×10^{-4}			[100]
$Ti_{50}Ni_{15}Cu_{25}Sn_3Be_7$			2170	~1.8		ϕ1 × 2	1×10^{-4}			[84]
$Ti_{45.8}Zr_{6.2}Cu_{39.9}Ni_{5.1}Sn_2Si_1$			~2000	5		ϕ2 × 4	2.1×10^{-4}			[104]
$Ti_{41.5}Zr_{2.5}Hf_5Cu_{42.5}Ni_{7.5}Si_1$			2080	<2		ϕ3 × 6	3×10^{-4}	103		[99]
$Ti_{47}Zr_{7.5}Cu_{40}Fe_{2.5}Sn_2Si_1$			>2000	1.5		ϕ2 × 4	2.1×10^{-4}	100		[55]
$Ti_{45}Cu_{25}Ni_{15}Sn_3Be_7Zr_5$			2480	~4		ϕ1 × 2	1×10^{-4}			[105]
$(Ti_{40}Zr_{25}Be_{20}Cu_{12}Ni3)_{99.5}Y_{0.5}$			1847	0		ϕ5 × 10	1×10^{-4}			[106]
$Ti_{46}Zr_{11.5}Cu_{31.5}Co_7Sn_3Si_1$		2477.9	2623.3	0.83		ϕ2 × 4				[126]

Table 4. *Cont.*

Composition (atom %)	Density (g/mm^3)	σ_y (MPa)	σ_{max} (MPa)	ε_p (%)	σ_c (N·m/kg)	Sample Size (mm)	Stain Rate (s^{-1})	*E* (GPa)	ν	Ref.
$Ti_{41.5}Zr_{2.5}Hf_5Cu_{37.5}Ni_{7.5}Si_1Sn_5$	7.0		2260	0.5	3.31×10^5	$\phi 3 \times 6$	4×10^{-4}	108		[54]
$Ti_{46}Cu_{27.5}Zr_{11.5}Co_7Sn_3Si_1Ag_4$	6.44	2126		1.03	3.30×10^5	$\phi 2 \times 4$	1×10^{-4}	97		[110]
$Ti_{47}Cu_{38}Zr_{7.5}Fe_{2.5}Sn_2Si_1Ag_2$	6.30	2010	2080	2.5	3.20×10^5	$\phi 2 \times 4$	2.1×10^{-4}	100		[56]
$Ti_{45}Cu_{40}Zr_{7.5}Fe_{2.5}Sn_2Si_1Sc_2$	6.27	2003	2150	5.9	3.20×10^5	$\phi 2 \times 4$	2×10^{-4}	97.1	0.362	[57]
$Ti_{44}Cu_{40}Zr_{7.5}Fe_{2.5}Sn_2Si_1Sc_3$	6.20	1963	2042	2.0	3.20×10^5	$\phi 2 \times 4$	2×10^{-4}	95.4	0.362	[57]
$Zr_{41.2}Ti_{13.8}Cu_{12.5}Ni_{10}Be_{22.5}$	6.07	1737	1774	1.0	2.92×10^5	$\phi 2 \times 4$		96	0.366	[53]
$Zr_{46.75}Ti_{8.25}Cu_{7.5}Ni_{10}Be_{27.5}$	5.99	1820	1890	2.0	3.04×10^5	ϕ 2 × 4		99.6	0.364	[53]
$Zr_{52.5}Ti_5Cu_{17.9}Ni_{14.6}Al_{10}$	6.55	1850	1900	2.0	2.82×10^5	$\phi 2 \times 4$		87.2	0.370	[53]
$Zr_{57}Cu_{15.4}Ni_{12.6}Al_{10}Nb_5$	6.68	1785	1800	0.5	2.67×10^5	$\phi 2 \times 4$		87.3	0.365	[53]
$Pd_{77.5}Cu_{6.0}Si_{16.5}$	10.59	1476	1600	11.4	1.39×10^5	$2 \times 2 \times 4$	4×10^{-4}	92.9	0.411	[146]
$Mg_{57}Cu_{31}Y_{6.6}Nd_{5.4}$	3.81	1126	1188	1.2	2.96×10^5	$\phi 1 \times 2$	1×10^{-4}	54.4	0.312	[17]
$Al_{86}Ni_7Y_{4.5}Co_1La_{1.5}$	3.14	1050		~4	3.34×10^5	$\phi 1 \times 2$	1×10^{-4}			[147]
Ti–6Al–4V	4.40	729 [a]	954 [a]		1.66×10^5			110–114	0.349	
AZ91	1.82	160 [a]	280 [a]		0.88×10^5			~45	~0.35	
7075-T6	2.81	503 [a]	572 [a]		1.79×10^5			71	~0.28	

σ_y: Yield strength; σ_{max}: ultimate strength; ε_p: plastic strain; σ_c: specific strength (defined as σ_y / ρ); *E*: Young's modulus; ν: Poisson's ratio. [a] Tensile data.

3.2. Strength and Ductility

As a typical class of light metal-based BMGs, the development of Ti-based BMGs has been closely linked with high specific strength. Table 4 lists the density and compressive mechanical properties of typical Ti-based BMGs together with other BMGs and crystalline lightweight alloys [40,41,45,47,49,52–57,72,79–82,84,86–95,99–106,110,126,145–147]. As shown in Table 4, Ti-based BMGs exhibit high yield strengths of 1700–2300 MPa, which is the same level as that of Zr-based BMGs and much higher than that of other light metal-based BMGs (e.g., Mg- and Al-based BMGs). For comparison, the yield strength of the Ti–6Al–4V alloy is 825–895 MPa, which is only about half that of Ti-based BMGs. Although the density of Ti is higher compared with Mg and Al, the specific strength σ_c of Ti-based BMGs is significantly higher, especially Be-containing Ti-based BMGs that possess densities of less than 5 g/cm^3 and high specific strength over 4×10^5 N·m/kg. Figure 10 shows the Ashby diagram of strength versus density for engineering materials [29]. It is clear that Ti-based BMGs possess higher specific strength than that of most other engineering materials. In order to further enhance the specific strength of Ti-based BMGs, the content of heavy constituent elements should be decreased without sacrificing the GFA. Unlike Fe- and Mg-based BMGs, which are completely brittle and fracture via fragmentation even under compression [151–153], most Ti-based BMGs exhibit a certain plastic strain and fracture mainly by shearing. This is mainly because of the relatively high Poisson's ratio of Ti and main constituent elements (e.g., Cu, Zr, and Pd). However, compared with Pd- and Zr-based BMGs, the room temperature plasticity of Ti-based is still relatively low.

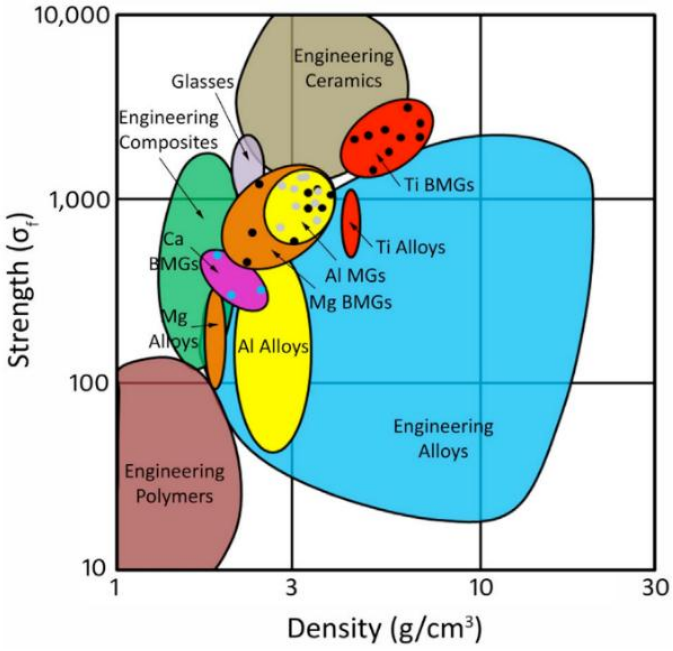

Figure 10. The Ashby diagram of strength versus density for engineering materials. Reproduced with permission from [29]. Copyright 2014, John Wiley and Sons.

Some scholars have also investigated the tensile properties of Ti-based BMGs. Figure 11 shows stress–strain curves of $Ti_{41.5}Cu_{42.5}Ni_{7.5}Zr_{2.5}Hf_5Si_1$ BMG obtained by tension and compression tests [99]. It was found that the tensile strength is slightly lower than the compressive strength. Moreover, although this Ti-based BMG exhibits certain ductility under compression, no plastic deformation is observed during the tension test. At room temperature, the plastic deformation of BMGs is dominated by localized shear bands. Under compression, the propagation of the primary shear band is restricted by the friction and confinement at the sample-loading platen surface. Then, multiple shear bands form and interact, leading to the substantial development of plastic deformation. However, this effect

is not available under tension. Under the unconfined tensile loading, once a shear band penetrates the sample and bears the entire load, catastrophic fracture will immediately occur. Therefore, it is more difficult to obtain tensile ductility for BMGs including Ti-based BMGs. Few Ti-based BMG matrix composites have exhibited tensile plasticity [154–156]. Developing Ti-based BMGs with tensile ductility is still a challenge.

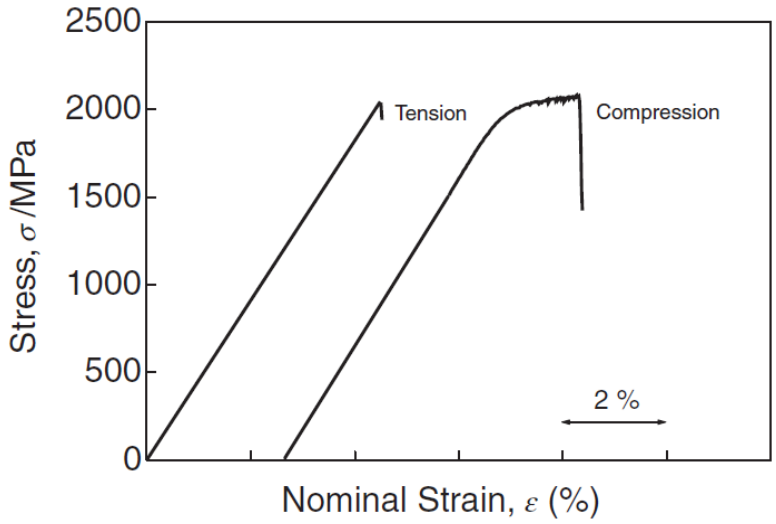

Figure 11. Stress–strain curves of BMG samples obtained by tension and compression tests. Reproduced with permission from [99]. Copyright 2004, The Japan Institute of Metals and Materials.

It is worthy noticing that sample size plays an important role on the plasticity of Ti-based BMGs. Huang et al. reported a "smaller is softer" phenomenon in $Ti_{40}Zr_{25}Ni_3Cu_{12}Be_{20}$ BMG under compression [157]. According to their experiments, Ti-based BMG samples with a smaller diameter exhibit a larger plasticity, while the strength does not markedly change. Similar results have also been reported in other BMGs [158–163]. The size effect has been explained from the viewpoints of free volume content [157,162,163], flaw sensitivity [159], plastic zone [160], and elastic energy dissipation [161]. Except for the sample diameter, the aspect ratio is another important size factor that affects the ductility of BMGs [164]. By decreasing the aspect ratio of BMG samples, the geometrical constrain effect becomes more obvious and the compressive plasticity can be dramatically improved.

It was also found that the compressive mechanical properties of Ti-based strongly depends on the service temperature. A transition from ductile to brittle behavior in $Ti_{40}Zr_{25}Ni_3Cu_{12}Be_{20}$ BMG at cryogenic temperatures has been reported by Huang et al. [165]. Because of the cryogenic surroundings, the diffusion of the atoms slows down, and the nucleation and growth of nanocrystals is suppressed, resulting in an improvement of both strength and plasticity.

3.3. Fracture Toughness

The lack of room temperature plasticity has been considered as the Achilles' heel of BMGs. In this section, typical techniques for improving the room temperature plasticity of Ti-based BMGs have been introduced.

3.3.1. Poisson's Ratio Control Strategy

Because of the correlation between the Poisson's ratio and plasticity, BMGs with good plasticity can be developed via composition optimization based on Poisson's ratio control strategy [166,167]. A simple but effective way is replacing one of the constituent elements with alloying elements that possess a higher Poisson's ratio. Gong et al. investigated the alloying effect on the compressive plasticity of Ti–Zr–Be BMGs [87–94]. Among the constituent elements in the Ti–Zr–Be system,

Be possesses a very low Poisson's ratio of 0.032, while Zr possesses a high Poisson's ratio of 0.34. Therefore, it is not surprising that replacing Be by alloying elements (e.g., Fe, Cu, Ni, and Al) in the Ti–Zr–Be BMG improves the plasticity, while the substitution of alloying elements to Zr degrades room temperature plasticity. Park et al. [53] also reported that partial substitution of Zr by Ti in the Ti–Cu–Ni–Be system increases the plastic strain from 0.7% to 8.3%. The addition of Zr is beneficial for increasing the Poisson's ratio and the shear transformation zone volume, resulting in larger plasticity.

3.3.2. Nanocrystallization

Producing BMG composites reinforced by ductile crystalline phases is believed to be an effective way to overcome the poor room temperature ductility of BMGs [168,169]. Table 5 summarizes the composition, synthesis method, and mechanical properties of typical Ti-based BMG composites [153,170–180]. It is found that most developed Ti-based BMG composites are of an in situ β-phase dendrite-reinforced type, as β-Ti possesses good ductility and a low modulus compared with hexagonal α-Ti. In general, Ti-based BMG composites exhibit better plasticity compared with Ti-based BMGs. For instance, Hofmann et al. developed Ti–Zr–V–Cu–Be BMG-matrix composites reinforced by a dendritic phase with room temperature tensile ductility over 10% [154,155]. However, the preparation process of BMG-matrix composites is always very complex [181]. The processing parameters should be precisely controlled to obtain a perfect microstructure. Therefore, the preparation of BMG composites puts a greater demand on the equipment. For example, a copper mold casting is the most widely used method of preparing BMGs. However, the microstructure of BMG composites prepared via copper mold casting is not always uniform because of the cooling rate difference. Zhang et al. [178] introduced a new technology named Bridgman solidification, which ensures the uniform microstructure of the prepared BMG composites by precisely controlling the processing parameters, but the corresponding equipment is more complex than traditional arc-melter. Moreover, the enhancement of ductility is always obtained at the price of lower strength. By introducing nanocrystals in situ formed in the glassy matrix, the propagation of primary shear band is disturbed when it reaches the nanocrystals, which act as high energy barriers; then, the primary shear band may be forced to be deflected and branched to initiate new shear bands. As a result, the ductility of BMGs can be improved without sacrificing strength. For example, Park et al. [121] reported a $Ti_{40}Zr_{29}Be_{14}Cu_9Ni_8$ BMG with a large plastic strain of ~7%. In order to find out the reason of the superior plasticity, they investigated the microstructure and crystallization behavior of this alloy with a high resolution transmission electron microscope (HRTEM) and via differential scanning calorimetry (DSC). It was found that, during the deformation, the nuclei transform to precipitations with a size of several nanometers and disperse into the amorphous matrix, resulting in an improvement in ductility. There are several different ways to introduce nanocrystallization in BMG samples. The first method is composition design. For instance, the addition of alloying elements may promote nanocrystallization of BMGs during the deformation process. Typical examples are Nb for Ti–Zr–Cu–Pd alloys [50] and Si for Ti–Zr–Cu–Ni–Sn alloys [104]. Another widely used method is annealing treatment. Jun et al. [182] reported that the compressive strain of $Ti_{43.3}Zr_{21.7}Ni_{7.5}Be_{27.5}$ BMG can be significantly enhanced to 42% after sub-T_g annealing. Nanocrystalline phases formed during the annealing were believed to be responsible for the rise of the compressive plastic strain. Moreover, as structural relaxation also occurs during the annealing process, the free volume content of the amorphous matrix decreases, which maintains the high strength of the annealed BMG samples.

Table 5. A brief summary of Ti-based bulk metallic glass composites [153,170–180].

Alloys (Atom %)	Reinforced Phase	Type	Synthesis Method	Density (g/mm^3)	Test Method	σ_y (MPa)	σ_{max} (MPa)	ε_p (%)	σ_c (N·m/kg)	Ref.
$Ti_{48}Zr_{20}V_{12}Cu_5Be_{15}$	BCC $Ti_{66}V_{19}Zr_{14}Cu_1$ dendrites	In situ	Arc melting	5.15	Tensile	1362	1429	10.2	2.64×10^5	[153]
$Ti_{50}Cu_{23}Ni_{20}Sn_7$	HCP-Ti dendrites + Ti_3Sn + β-(Cu, Sn)	In situ	Arc melting & Cu mold casting		Compression	1190	2130	6		[170]
$Ti_{52.9}Zr_{34.5}Ni_{1.6}Cu_{4.2}Be_{6.8}$	BCC $Ti_{61.5}Zr_{36.4}Cu_{2.1}$ dendrites	In situ	Arc melting & Cu mold casting		Compression	1243	1919	10.7		[171]
$Ti_{50}Zr_{20}Nb_{12}Cu_5Be_{13}$	B-Ti(Zr, Nb) dendrites	In situ	Arc melting & copper mold casting		Compression	1839	2425	>21		[172]
$Ti_{43.2}Cu_{38}Ni_{10}Zr_{7.8}Al_{0.5}Si_{0.5}$	B2-(Ti, Zr)(Cu, Ni) dendrites	In situ	Arc melting & Cu mold casting		Compression	1255	2960	16.5		[173]
$Ti_{56}Zr_6Cu_{19.8}Pd_{8.4}Sn_{1.8}Nb_8$	Nb-rich β-Ti dendrites	In situ	Arc melting & Cu mold casting		Compression	1690	2680	20		[174]
$Ti_{34.3}Zr_{21.6}Ni_{4.6}Cu_{8.5}Be_{17}Nb_{15}$	β-Ti dendrites	In situ	Arc melting & Cu mold casting		Compression	1720	1790	25		[175]
$(Ti_{58}Ni_{28}Cu_8Si_4Sn_2)_{94}Mo_6$	β-Ti dendrites	In situ	Arc melting & Cu mold casting	6.54	Compression	1134	2372	12.18	1.73×10^5	[176]
$(Ti_{38.8}Zr_{28.8}Cu_{6.2}Be_{16.2}Nb_{10})_{92}Ta_8$	BCC β(Ti, Zr)(Nb, Ta) dendrites	In situ	Arc melting & copper mold casting		Compression	815	2032	27.2		[177]
$Ti_{46}Zr_{20}V_{12}Cu_5Be_{17}$	β-TiZr dendrites	In situ	Arc melting & Bridgman solidification		Compression	1956	2706	15.3		[178]
$Ti_{47}Zr_{19}Be_{15}V_{12}Cu_7$	β-Ti dendrites	In situ	Arc melting & Bridgman solidification		Compression	1601	3024	32.6		[179]
$Ti_{42.5}Cu_{40}Zr_{7.5}Ni_5Sn_5$	Diamond	Ex-situ	Spark plasma sintering		Compression		1850	0		[180]

3.3.3. Pre-Plastic Deformation

For conventional crystalline alloys, after plastic deformation, the microstructure can be changed (e.g., dislocation density), and the flow behaviors can be quite different. For BMGs, pre-plastic deformation is supposed to introduce microstructural inhomogeneities and induce controlled stress distributions or activate multiple shear bands, which are beneficial to enhancing the room temperature plasticity [183,184]. Huang et al. utilized prior compressive plastic deformation to tune the room temperature plasticity of $Ti_{40}Zr_{25}Ni_3Cu_{12}Be_{20}$ BMG [185]. It was found that, with the increase of prior plastic strain, the plastic strain of the deformed BMG samples first increases and then decreases with the optimized prior plastic strain of 10%. The improvement of compressive plasticity was explained in view of the free volume content. Park et al. [186] investigated the effect of strain-induced internal state modulation created by cold rolling on the compressive plasticity of $Ti_{40}Zr_{25}Ni_8Cu_9Be_{18}$ BMG. The compressive plastic strain can be dramatically improved from 1.5% to 14.5% with a 50% thickness reduction (as shown in Figure 12). Because of rolling, a network-like structure of hard and soft regions was found to be introduced uniformly in the BMG samples, which is beneficial to the uniform distribution of multiple shear bands.

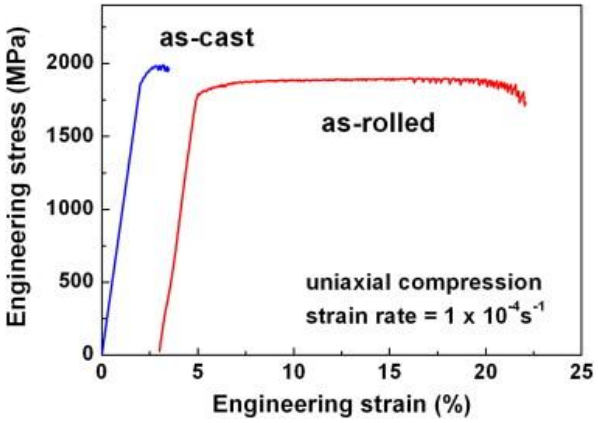

Figure 12. Compressive stress–strain curves of as-cast and cold-rolled $Ti_{40}Zr_{25}Ni_8Cu_9Be_{18}$ BMG samples. Reproduced with permission from [186]. Copyright 2012, Elsevier.

3.3.4. Surface Treatment

Surface treatment has been widely applied to improve the room temperature ductility of BMGs by retarding the initiation and propagation of the shear band [187]. It has been reported that the room temperature plasticity of Zr-based BMGs can be improved by various surface modification technologies including shot peening [188] and surface coating [189,190]. As Ti-based BMGs possess properties similar to Zr-based BMGs, these strategies can also be adopted to improve the room temperature plasticity of Ti-based BMGs. Fan et al. [191] proposed a novel technology called surface mechanical attrition treatment (SMAT) to improve the plasticity of BMGs. By surface crystallization, isolated crystallite islands are formed in the top surface layer, which act as the obstacles to restrict the localization of shear bands and avoid the development of cracks. With the optimization of SMAT processing parameters, the plastic strain of $Ti_{40}Zr_{25}Ni_3Cu_{12}Be_{20}$ BMG can be enhanced to 3.78%, which is nearly four times that of the untreated sample.

3.4. Fracture Toughness

For engineering materials, damage tolerance is a very important mechanical design parameter. As BMGs usually possess high strength but a lack of plasticity, fracture toughness K_c, which assesses a material's resistance to crack propagation and can be measured by the energy needed to cause fracture, is a more important indicator of mechanical performance compared with yield strength [192].

The fracture toughness of BMGs strongly depends on the alloy composition. For instance, some brittle BMGs (e.g., Mg- and Fe-based BMGs) exhibit an ideally brittle behavior (K_c < 10 MPa·m$^{1/2}$) [193,194], while Pd-based BMGs are remarkably tough (K_c ~200 MPa·m$^{1/2}$) [195]. Regarding the fracture toughness of Ti-based BMGs, it has been reported that the K_c of $Ti_{50}Ni_{24}Cu_{20}B_1Si_2Sn_3$ alloy is ~50 MPa·m$^{1/2}$ [153]. Gu et al. [196] investigated the effects of changes in sample dimensions and the stress state on the fracture toughness of $Ti_{40}Zr_{25}Cu_{12}Ni_3Be_{20}$ BMG. It was found that the measured fracture toughness ranges from 98.6 to 126.3 MPa·m$^{1/2}$. The fatigue pre-cracked $Ti_{40}Zr_{25}Cu_{12}Ni_3Be_{20}$ sample exhibited a slightly higher toughness than that of the notched sample. The notched plate sample and the notched rod sample were also found to have different fracture toughness values. In summary, the fracture toughness of Ti-based BMGs is higher than that of brittle BMGs but lower than that of Pd-BMGs, which is comparable to those for age-hardened Al-based alloys (24–36 MPa·m$^{1/2}$), commercial Ti crystalline alloys (K_c = 54–98 MPa·m$^{1/2}$), and 4340 high strength steels (K_c ~ 50 MPa·m$^{1/2}$). However, it should be noticed that, even for the same alloy, a wide scatter in K_c has been reported. The cooling rate during the preparation process, the stress state, the impurity inclusions, the sample size, and the sharpness of notch/crack fabrication are all possible reasons. In order to reduce the extrinsic effect, Chen et al. [197] proposed a novel sample preparation method for fracture toughness test via the thermoplastic forming of BMGs and Si photolithography. Using this strategy, they measured the notch toughness of 86 ± 3 MPa·m$^{1/2}$ for a $Ti_{41}Zr_{25}Be_{28}Fe_6$ BMG. The small scatter is believed to reflect an intrinsic origin rather than extrinsic sample preparation effects.

3.5. Fatigue Properties

The fatigue behavior is one of the dynamic mechanical properties and also a very important characteristic for the applications of BMGs as structural materials. Yamaura et al. [198] and Fujita et al. [199] have investigated the fatigue behavior of $Ti_{40}Zr_{10}Cu_{34}Pd_{14}Sn_2$ and $Ti_{41.5}Zr_{2.5}Hf_5Cu_{42.5}Ni_{7.5}Si_1$ alloys, respectively. Table 6 lists the fatigue properties of Ti-based BMGs together with other typical BMGs and Ti–6Al–4V alloy [198–202]. Compared with the Ti–6Al–4V alloy, $Ti_{40}Zr_{10}Cu_{34}Pd_{14}Sn_2$ BMG, which is a typical representative of biomedical Ti-based BMG, exhibits higher fatigue strength although the fatigue ratio is lower. Moreover, it is worthy noticing that the $Ti_{41.5}Zr_{2.5}Hf_5Cu_{42.5}Ni_{7.5}Si_1$ BMG shows a fatigue ratio of 0.79, which is significantly higher than that of other BMGs such as Zr-, Cu-, Co-, and Fe-based BMGs listed in Table 6. The fatigue strength of $Ti_{41.5}Zr_{2.5}Hf_5Cu_{42.5}Ni_{7.5}Si_1$ BMG is up to 1610 MPa, which is much larger than that of Zr-based BMGs and close to the value of Ni–based BMGs. The superior fatigue properties of $Ti_{41.5}Zr_{2.5}Hf_5Cu_{42.5}Ni_{7.5}Si_1$ BMG are attributed to the dispersion of nano-scaled crystalline particles in the glassy matrix. The initiation and the growth of shear bands are constrained by the nanocrystals. The shear bands branch, kink, and rotate, resulting in the reduction in the shear stress value near their tips. There have been few reports on the effect of frequency on the fatigue properties of Ti-based BMGs, and this will need to be further studied.

Table 6. Fatigue-endurance limits and fatigue ratios of various BMGs [198–202].

Composition (Atom %)	Ultimate Tensile Strength (MPa)	Fatigue Endurance Limit (MPa)	Fatigue Ratio	Frequency (Hz)	R	Ref.
$Ti_{40}Zr_{10}Cu_{34}Pd_{14}Sn_2$	2050	762	0.37	20000	AX *-1	[198]
$Ti_{41.5}Zr_{2.5}Hf_5Cu_{42.5}Ni_{7.5}Si_1$	2040	1610	0.79	10	AX 0.1	[199]
$Zr_{50}Al_{10}Cu_{40}$	1821	752	0.41	10	AX 0.1	[200]
$Zr_{50}Al_{10}Cu_{30}Ni_{10}$	1900	865	0.46	10	AX 0.1	[200]
$Zr_{41.2}Ti_{13.8}Cu_{12.5}Ni_{10}Be_{22.5}$	1850	703	0.38	10	AX 0.1	[200]
$[(Co_{0.6}Fe_{0.4})_{0.75}B_{0.2}Si_{0.05}]_{96}Nb_4$	4170	2370	0.57	10	AX 0.1	[200]
$(Fe_{0.5}Co_{0.5})_{72}B_{20}Si_4Nb_4$	4200	2280	0.54	10	AX 0.1	[200]
$Ni_{60}Zr_{20}Nb_{15}Al5$	2900	1680	0.58	10	AX 0.1	[200]
$Cu_{60}Zr_{30}Ti_{10}$	2000	980	0.49	10	AX 0.1	[199,201]
Ti–6Al–4V	960	535	0.56	20000	AX-1	[202]

* AX: Axial Loading.

3.6. Thermoplastic Formability

BMGs usually present superplasticity in their supercooled liquid region with behavior similar to a Newtonian viscosity of conventional glass materials. Because of this unique property, thermoplastic forming (TPF) and patterning have been widely used to precisely fabricate BMG parts on length scales ranging from the nanometer scale to several centimeters [203–205]. There are two key factors influencing the thermoplastic formability of BMGs: the temperature-dependent viscosity and the temperature-dependent crystallization time. It was already known that the temperature dependence of the viscosity and the temperature dependence of crystallization time among BMGs vary significantly. Thus, the thermoplastic formability of BMGs strongly depends on the alloy composition. Schroers et al. [206] introduced an experimental method to characterize the thermoplastic formability of different BMGs using the maximum diameter to which the BMG can be deformed for a standardized set of processing parameters. It was found that the S parameter, which is defined based on the characteristic temperatures ($S = \Delta T_x/T_l - T_g$), is the best indicator for thermoplastic formability of BMGs so far. Table 7 summarizes the S values of developed Ti-based BMGs together with some typical Zr-, Pd-, Pt-, Au-, Fe-, and Mg-based BMGs [39,40,47,54,56,79,84,86,95,206–212]. It is found that Ti-based BMGs possess relatively small S values compared with other BMGs, implying a relatively low thermoplastic formability. Moreover, as titanium is a very active element, during the heating process in air, the oxidation is more serious compared with Pd-, Au-, and Pt-based BMGs, which is harmful to the thermoplastic forming [213–215]. In order to perform the thermoplastic forming of Ti-based BMGs, especially in air, it is necessary to first attempt composition optimization in order to develop novel Ti-based BMGs with better thermoplastic formability and oxidation resistance. Be alloying may be an effective way as Be-containing Ti-based BMGs possess relatively higher S value (as shown in Table 7). Other strategies, e.g., vibrational loading [216] or introducing a wetting layer [217], are also recommended.

Table 7. Thermoplastic formability of typical Ti-based BMGs together with various BMG forming alloys [39,40,47,54,56,79,84,86,95,206–212].

Composition (Atom %)	*S* Parameter	Ref.
$Ti_{50}Zr_{42}Ni_8$	0.11	[40]
$Ti_{45}Zr_{20}Be_{35}$	0.11	[79]
$Ti_{40}Zr_{10}Cu_{36}Pd_{14}$	0.10	[86]
$Ti_{40}Zr_{10}Cu_{34}Pd_{14}Sn_2$	0.10	[47]
$Ti_{42.5}Zr_{7.5}Cu_{40}Ni_5Sn_5$	0.12	[95]
$Ti_{50}Ni_{15}Cu_{25}Sn_5Zr_5$	0.10	[39]
$Ti_{40}Zr_{25}Ni_8Cu_9Be_{18}$	0.12	[84]
$Ti_{41.5}Zr_{2.5}Hf_5Cu_{37.5}Ni_{7.5}Si_1Sn_5$	0.13	[54]
$Ti_{47}Cu_{38}Zr_{7.5}Fe_{2.5}Sn_2Si_1Ag_2$	0.10	[56]
$Pd_{43}Ni_{10}Cu_{27}P_{10}$	0.31	[206,207]
$Pt_{57.5}Cu_{14.7}Ni_{5.3}P_{22.5}$	0.34	[206,208]
$Au_{49}Ag_{5.5}Pd_{2.3}Cu_{26.9}Si_{16.3}$	0.24	[206,209]
$Zr_{41.2}Ti_{13.8}Ni_{10}Cu_{12.5}B_{22.5}$	0.21	[206,210]
$Zr_{44}Ti_{11}Cu_{10}Ni_{10}Be_{25}$	0.25	[206,211]
$Mg_{65}Cu_{25}Y_{10}$	0.19	[212]

4. The Corrosion Resistance of Ti-Based BMGs

Due to the formation of stable and protective surface oxide film, titanium alloys are inert and resistant to corrosion. Because of the potential application as structural and biomedical materials, the corrosion behavior of Ti-based BMGs in different solutions such as acid, alkaline, salt, and simulated body solutions have been investigated. Compared with conventional Ti alloys, Ti-based BMGs always exhibit better corrosion resistance in different kinds of solutions because of the unique amorphous structure. Figure 13 [110] shows the potentiodynamic polarization curves of

$Ti_{46}Cu_{27.5}Zr_{11.5}Co_7Sn_3Si_1Ag_4$ BMG and Ti–6Al–4V alloys in PBS, 0.9 wt. % NaCl, 1 mol/L HCl, and 1 mol/L NaOH solutions, respectively. It was found that, compared with the commercial Ti–6Al–4V alloy, $Ti_{46}Cu_{27.5}Zr_{11.5}Co_7Sn_3Si_1Ag_4$ BMG possesses a higher corrosion potential and lower corrosion current density, implying a better corrosion resistance. In general, the corrosion-penetration rates (CPRs) of less than ~76 μm/year are considered acceptable for chemical and industrial applications. According to Morrison et al.'s research [218], the CPR of $Ti_{43.3}Zr_{21.7}Ni_{7.5}Be_{27.5}$ BMG in a PBS electrolyte at 37 °C is 2.9 ± 2.6 μm/year, which is well within the expected range for corrosion resistant materials and equivalent to, or better than, Zr-based BMGs and 316L stainless steel. Except for PBS, Ti-based BMGs also exhibit good bio-corrosion resistance in other simulated body fluids such as SBF, Ringer's solution, and Hanks' solution [219].

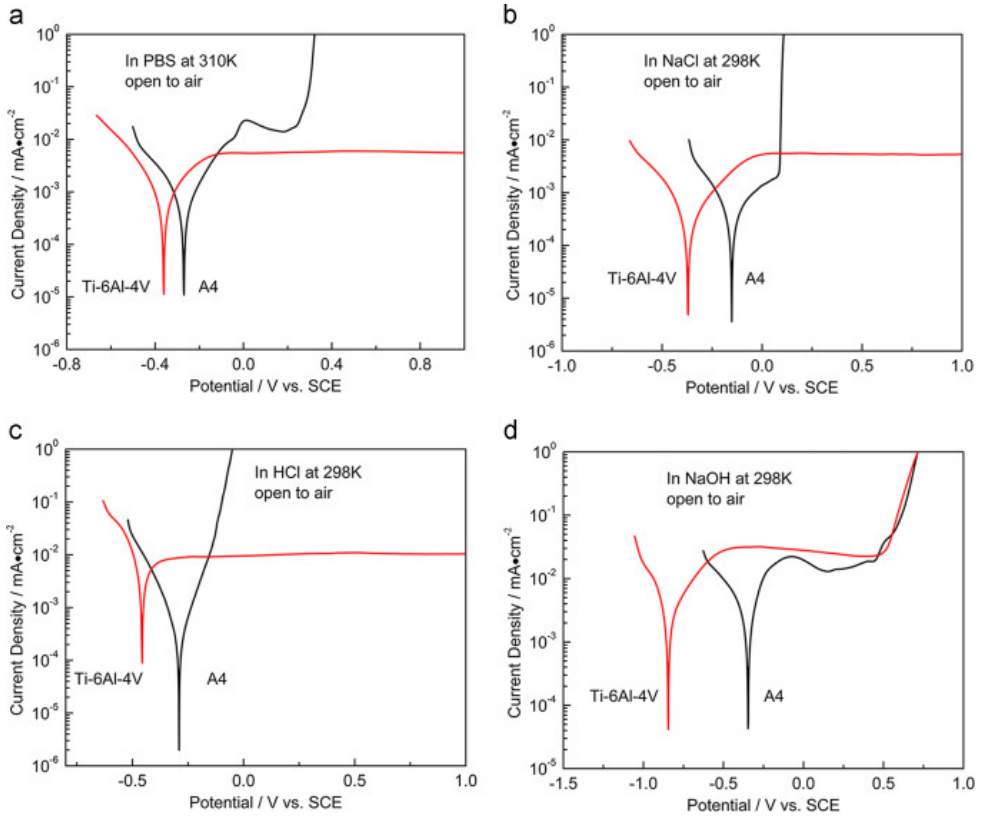

Figure 13. Potentiodynamic polarization curves of BMG and the Ti–6Al–4V alloy in (**a**) PBS, (**b**) 0.9 wt % NaCl, (**c**) 1 mol/L HCl, and (**d**) 1 mol/L NaOH solutions. Reproduced with permission from [110]. Copyright 2015, Elsevier.

Chemical composition also plays an important role on the corrosion resistance of Ti-based BMGs. Qin et al. [220] investigated the effects of different alloying elements on the corrosion behavior of $Ti_{47.5}Cu_{42.5}Ni_{7.5}Zr_{2.5}$ BMG in a 0.14 kmol/m^3 NaCl solution and a 0.2 kmol/m^3 phosphate buffer solution with 0.14 kmol/m^3 Cl^- ions. It was found that the addition of Nb or Ta significantly improves corrosion resistance. The passive current density of the Nb- or Ta-containing BMGs is between 10^{-2} and 10^{-3} A/m, which is one order of magnitude lower than that of the base alloy. The addition of Nb or Ta facilitates the enrichment of Ti, and certain amounts of Nb or Ta existing in the surface film, resulting in higher corrosion resistance. The corrosion resistance of the $(Ti_{40}Zr_{10}Cu_{38}Pd_{12})_{97}Nb_3$ BMG has also been shown to be higher than that of the $Ti_{40}Zr_{10}Cu_{38}Pd_{12}$ alloy due to the presence of Nb. The pitting resistance is enhanced by the addition of Nb because of the improvement of the passive layer properties.

The effect of crystallization on the corrosion resistance of Ti-based BMGs has also been studied. Qin et al. [221] investigated the corrosion behavior of the $Ti_{40}Zr_{10}Cu_{36}Pd_{14}$ alloy in Hanks' solution in three different conditions: in the as-cast fully amorphous condition, after annealing it for 10 min at 723 K to obtain BMG matrix composite, and after fully crystallizing the sample at 823 K for 10 min. As shown in Figure 14, it was found that the as-cast and partially crystalline samples have lower passive current densities located ~10^{-2} A/m^2, markedly lower than that of the commercial Ti–6Al–4V alloy and pure Ti. However, the fully crystallized sample exhibits a much lower pitting potential, implying the least corrosion resistance. The enhancement of the pitting potential of the partially nanocrystalline alloy annealed at 723 K may be due to the formation of the Ti_3Cu_4 phase. This results in the enrichment of Pd in the matrix, which is helpful in forming a protective passive film. Moreover, because of the large number of interface defects that are expected at the nano scale, the breakdown of the passive film is uniform, which allows the partially crystallized alloy to maintain passivity. Correspondingly, the crystalline phases of the fully crystallized sample are Ti_3Cu_4, Ti_2Pd, and Ti_2Pd_3 with a larger size. The lower corrosion resistance is mainly attributed to the serious micro-galvanic corrosion between the Cu-rich and Pd-rich phases. In conclusion, both the size and composition of the crystalline phase play important roles in controlling the corrosion behavior of Ti-based alloys.

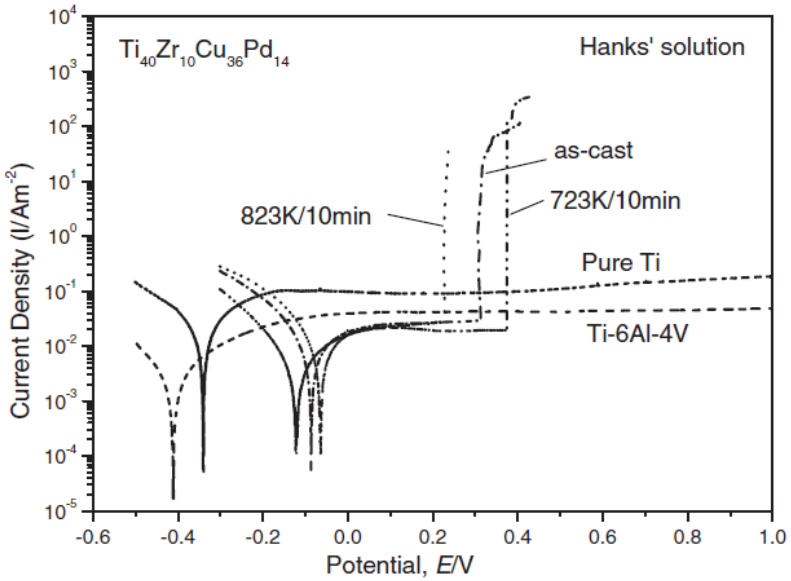

Figure 14. Anodic and cathodic polarization curves of the $Ti_{40}Zr_{10}Cu_{36}Pd_{14}$ BMG and its crystalline alloys at 310 K in Hanks' solution. Reproduced with permission from [221]. Copyright 2007, The Japan Institute of Metals and Materials.

5. Biocompatibility of Ti-Based BMGs

Titanium and its alloys are believed to be excellent implant materials in the fields of trauma and orthopedic surgery. Compared with conventional Ti alloys, Ti-based BMGs are more suitable for biomedical applications for the following reasons [222,223]: (1) high strength and hardness, which may lead to good loadbearing capability and high wear resistance; (2) low Young's (elastic) modulus, which implies better load transfer to the surrounding bone and a potential for mitigating stress-shielding; (3) excellent corrosion resistance, resulting in reduced ion release in the human body environment; and (4) excellent thermoplastic formability that allows for the production of precise and versatile geometries on different length scales, which is of great interest for biomaterials processing.

Young's modulus is one of the most important performance indicators of biomedical materials. According to Table 4, the Young's modulus value of Ti-based BMGs is 80–110 GPa, which is smaller than commercial biomedical materials such as biomedical 316L stainless steel (230 GPa), Co–Cr alloys

(230 GPa), and the Ti–6Al–4V alloy (110–114 GPa). However, the Young's modulus of human bone tissue is only 20 GPa, which is still much smaller than that of Ti-based BMGs. Some developed β-type titanium alloys (e.g., Ti–Nb–Ta–Zr) possess relatively small Young's modulus values of ~40 GPa [224], which are close to that of human bone tissue. In order to minimize the stress shielding effect, it is still necessary to decrease the Young's modulus value of biomedical Ti-based BMGs. In order to improve the GFA, Ti-based BMGs always contain several alloying elements. As the Young's modulus of BMGs shows a rough correlation with a weighted average of the Young's modulus for the constituent elements [225], the elements with a low Young's modulus value should be selected preferentially as constituent elements for biomedical Ti-based BMGs. On the other hand, the biological toxicity of different alloying elements has also been considered. Calin et al. investigated the biological safety of the constituent elements in Ti-based BMGs. Based on their research, it was concluded that Ti, B, Mg, Si, P, Ca, Sr, Zr, Nb, Mo, Pd, In, Sn, Ta, Pt, and Au are biocompatible elements, while harmful elements include Be, Al, V, Cr, Mn, Fe, Co, Ni, Cu, Zn, and Ag [223]. In this sense, Ti-based BMGs for biomedical use should only contain biocompatible and low-modulus elements. According to this principle, a series of Ti–Zr–Si–(Nb, Ta) metallic glasses that contain no harmful elements has been successfully developed [226,227]. However, the GFA of this class of Ti-based alloys is too poor to form BMG samples. No Ti-based BMGs that do not contain either Ni, Cu, or Be has been reported. It is known that Cu ions are necessary nutrients for the human body, but excess Cu ions may lead to biological toxicity. An amount of 10–12 mg per day may possibly be the maximally safe concentration, which is suggested by the World Health Organization. According to Huang et al.'s research, after 1 day of immersion in a cell culture medium (DMEM), the concentration of Cu ions released from $Zr_{50}Cu_{43}Al_7$ BMGs was below 50 ppb [228]. The addition of Cu in Ti-based BMGs results in no bio-toxicity. Similarly, a small amount of Fe, Ag, or both may also be added to Ti-based BMGs. Thus, Ti–Zr–Cu–Pd–(Sn, Nb) [47,49,86] and Ti–Zr–Cu–Fe–Sn–Si–(Ag) BMGs [56,57], potential biomaterials, were successfully discovered.

Biocompatibility is described as the ability of the material to exist in contact with tissues of the human body without causing a non-acceptable degree of harm. As a typical class of non-degradable BMGs, the biocompatibility of Ti-based BMGs can be mainly related to its cell-biological activity in the body environment. Wang et al. [229] studied the biocompatibility of $Ti_{41.5}Zr_{2.5}Hf_5Cu_{37.5}Ni_{7.5}Si_1Sn_5$ BMG and pure Ti via in vitro cell response and in vivo animal implants. It was found that, although the cell viability is relatively lower due to the release of Cu ions, $Ti_{41.5}Zr_{2.5}Hf_5Cu_{37.5}Ni_{7.5}Si_1Sn_5$ BMG shows good compatibility from in vivo evaluation for one month implantation compared with pure Ti. As shown in Figure 15, both the pure Ti and $Ti_{41.5}Zr_{2.5}Hf_5Cu_{37.5}Ni_{7.5}Si_1Sn_5$ BMG are well integrated with the bone tissue, and the gap between the bone tissue is no more than 5 μm. However, because of the high content of Cu and the addition of allergenic element Ni, $Ti_{41.5}Zr_{2.5}Hf_5Cu_{37.5}Ni_{7.5}Si_1Sn_5$ is not an ideal biomaterial, and long-term implantation is still needed for further investigation. Liu et al. [55] investigated the cytocompatibility of Ti–Zr–Cu–Fe–Sn–Si BMGs and the Ti–6Al–4V alloy via adopted mouse MC3Ts-E1 pre-osteoblast. The results demonstrated that the cell viabilities in the Ti–Zr–Cu–Fe–Sn–Si BMG extracts are slightly higher than that in the Ti–6Al–4V alloy extract. Kokubun et al. [230] conducted a thorough in vivo evaluation of biocompatibilities of $Ti_{40}Zr_{10}Cu_{34}Pd_{14}Sn_2$ BMG. They implanted bars of $Ti_{40}Zr_{10}Cu_{34}Pd_{14}Sn_2$ BMG in the femoral bone of rats. A typical macroscopic view of the $Ti_{40}Zr_{10}Cu_{34}Pd_{14}Sn_2$ bar at 12 weeks after implantation is shown in Figure 16. No inflammatory reaction, implant dislocation, or loosening was observed, implying that $Ti_{40}Zr_{10}Cu_{34}Pd_{14}Sn_2$ BMG has an excellent biocompatibility and integration to bone tissue. As shown in Figure 17, the histological images revealed that both the BMG sample and the Ti sample were well covered by surrounding bone tissue. No abnormal finding in surrounding bone tissue was observed, and no component ion diffusion was detected up to 3 months post-implantation.

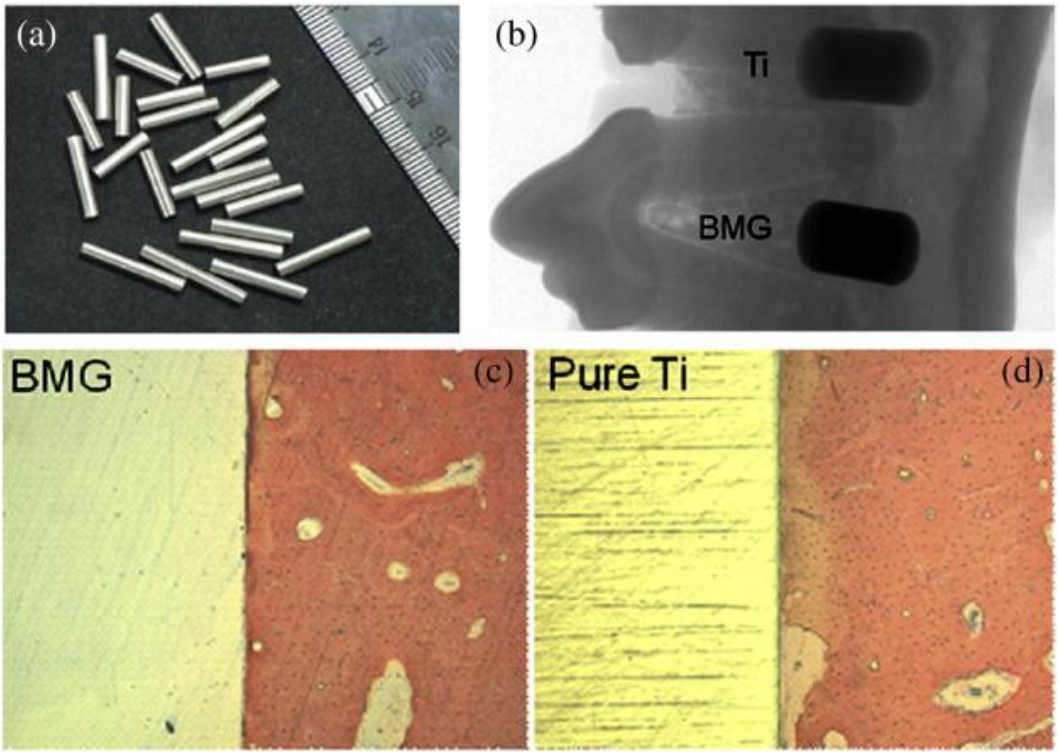

Figure 15. Implantation of $Ti_{41.5}Zr_{2.5}Hf_5Cu_{37.5}Ni_{7.5}Si_1Sn_5$ BMG and pure Ti samples. (**a**) BMG sample; (**b**) representative X-ray images for the implants; (**c**,**d**) representative histological images stained by methylene blue after 1 month of implantation [229]. Reproduced with permission from [229]. Copyright 2013, Elsevier.

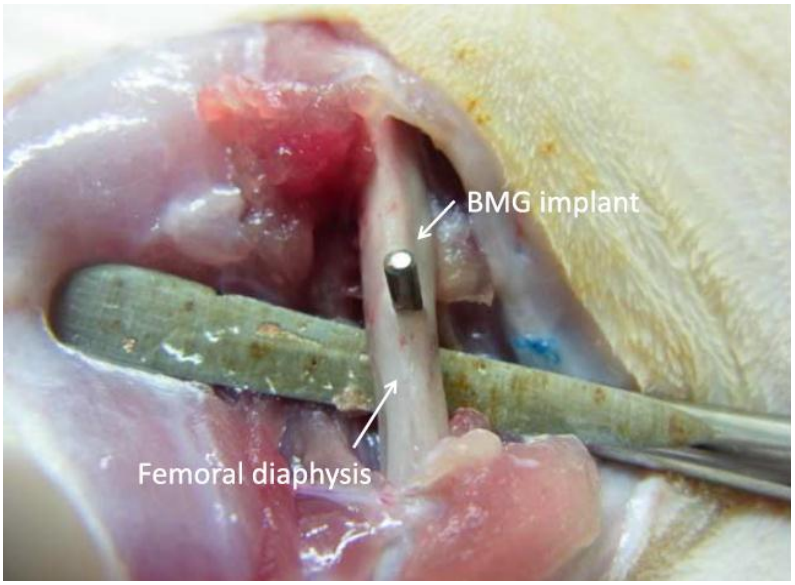

Figure 16. Macroscopic view of the $Ti_{40}Zr_{10}Cu_{34}Pd_{14}Sn_2$ BMG sample at 12 weeks after implantation in femoral diaphysis. Reproduced with permission from [230]. Copyright 2015, IOS press.

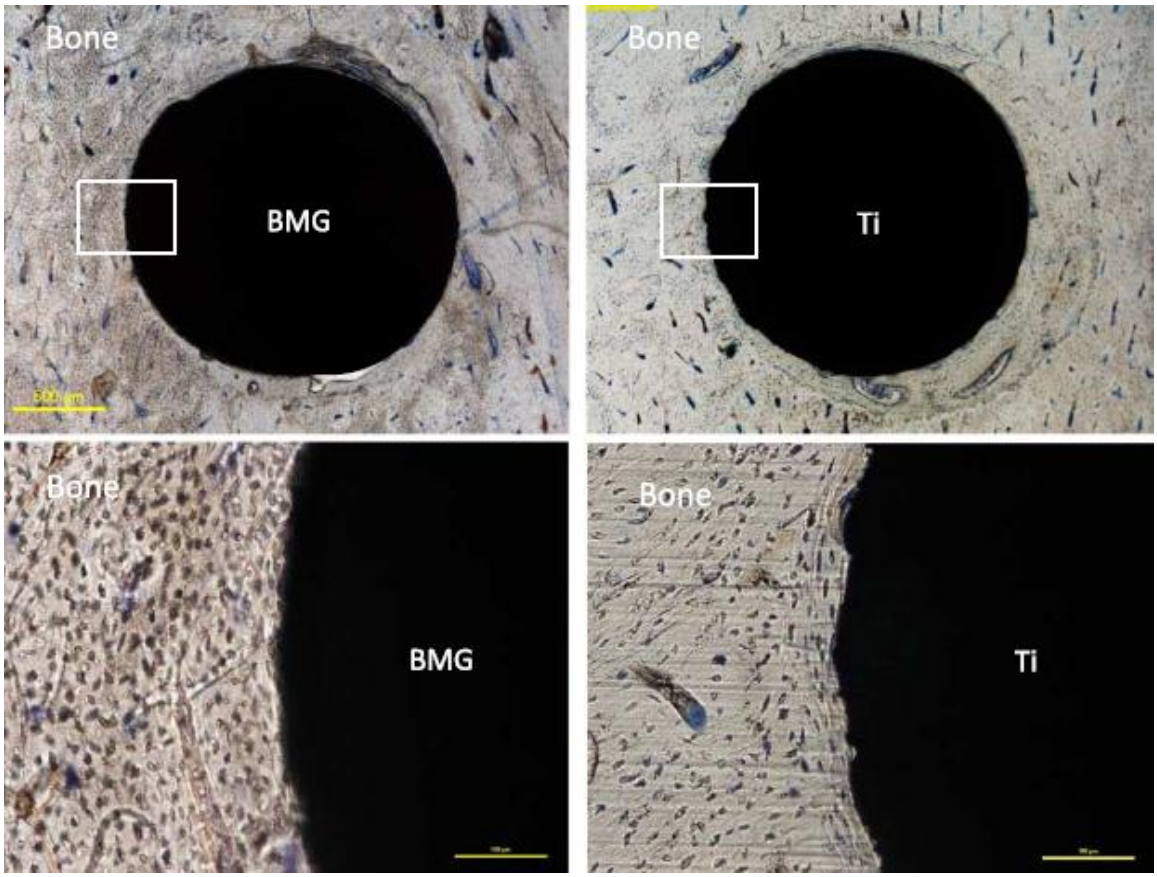

Figure 17. Histological views of Ti-based BMG implant and Ti implant. Both samples are well covered by surrounding bone tissue. Objective magnification of upper images is ×4, and that for lower images is ×20. Reproduced with permission from [230]. Copyright 2015, IOS press.

Based on the above experimental results, the possibility and efficacy of its use for bone implant is preliminarily confirmed. However, further long-term implant study is still recommended. Another issue is that the number of developed Ti-based BMGs for biomedical applications is very limited. It is still necessary to explore novel biomedical Ti-based BMGs with improved GFA and good biocompatibility.

6. Applications of Ti-Based BMGs

Ti-based BMGs have been applied to fabricate a sensing tube in a Coriolis flow meter, which is used to measure the Coriolis force of a liquid or gas that is flowing inside the pipe subjected to reinforced oscillation (as shown in Figure 18) [231,232]. A Ti-based BMG with the composition of $Ti_{50}Cu_{25}Ni_{15}Zr_5Sn_5$ was selected to fabricate the metallic glass tubes using a copper mold suction casting technique. The sensitivity of the Coriolis flow meter using the Ti-based glassy alloy pipe was reported to be 28–53 times higher than that of a conventional Coriolis flow meter using a SUS316 pipe. The significant improvement in sensitivity allows the possibility of the use of a new type of Coriolis flow meter in various industries such as fossil-fuel, chemical, environmental, semiconductor, and medical science fields.

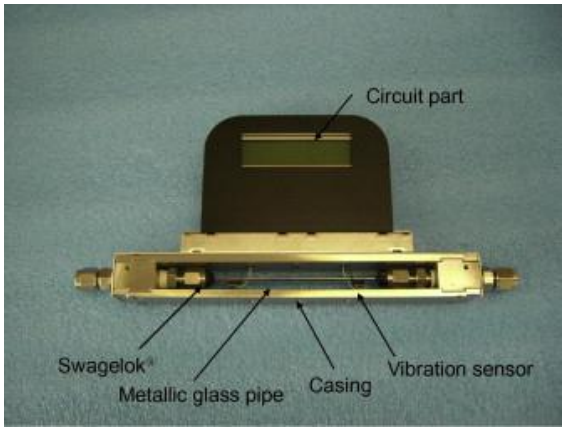

Figure 18. An outer appearance of the self-made Coriolis flow meter using the Ti–Cu–Ni–Zr–Sn BMG pipe. Reproduced with permission from [232]. Copyright 2011, Elsevier.

Ti-based BMGs are also potentially useful in many other serious applications. It was reported that Zr-based BMGs have been used to fabricate micro-geared motor parts [231–234], pressure sensors [231,235,236], watch cases [204,237], cell phone cases [204,237], and sports goods (e.g., golf plate) [238]. Replacing Zr-based BMGs by Ti-based BMGs is beneficial for enhancing the specific strength and reducing the cost. Because of the good corrosion resistance and biocompatibility, Ti-based BMGs are also suitable for medical components such as prosthetic implants and surgical instruments (e.g., the surgical razor and micro-surgery scissors). Aerospace engineering is another important applied field of Ti-based BMGs. Ti-based BMGs possess outstanding mechanical properties such as high specific strength, high hardness, and large elastic elongation. Moreover, although BMGs are metastable in thermodynamics, Ti-based BMGs exhibit high space environment applicability. According to Wang et al.'s experimental results [239], the microstructure, thermodynamics, and mechanical properties of Ti-based BMGs are all relatively stable after simulated thermal cycling treatment in vacuum in a temperature range of −196 °C to 150 °C. The effect of atomic oxygen (AO) on the BMGs has been also studied in a plasma type ground-based AO effect simulation facility. The results show that the structure on the surfaces of Ti-based BMGs samples do not change much, suggesting that Ti-based BMGs have high AO erosion resistance [240]. The combination of good mechanical properties and high space environment applicability implies that Ti-based BMGs possess a potential for applications in aerospace environments.

7. Conclusions and Future Research Directions

Ti-based BMGs have attracted much attention due to the combination of unique properties such as high specific strength and good anti-corrosion properties. In recent decades, many Ti-based BMGs have been successfully developed, and their GFA, mechanical properties, corrosion resistance, and biocompatibility have been investigated. In this paper, the development of Ti-based BMGs is reviewed. In terms of GFA, a maximum diameter for glass formation of over 50 mm is now achieved in $(Ti_{36.1}Zr_{33.2}Ni_{5.8}Be_{24.9})_{91}Cu_9$ and $Ti_{32.8}Zr_{30.2}Cu_9Fe_{5.3}Be_{22.7}$ alloys. In the aspect of mechanical properties, Ti–Be-based BMGs possess very high specific strength over 4×10^5 N·m/kg, which is more than twice that of the Ti–6Al–4V alloy. Because of the relatively high Poisson's ratio of titanium, Ti-based BMGs are classified as "ductile", and most developed Ti-based BMGs possess a certain plastic strain under compression. Ti-based BMGs also exhibit excellent corrosion resistance in acid, alkaline, and salt solutions compared with crystalline Ti alloys and typical engineering materials such as 316L stainless steel. Ti–Zr–Cu–Pd–(Sn, Nb) BMGs do not contain noxious elements and show good GFA together with a high potential for biomedical applications.

Although rapid progress has been made, several challenges for future applications of Ti-based BMGs still exist, including the need to (1) understand the glass-forming mechanisms and further improve the GFA of Ti-based BMG especially non-toxic, low-modulus, and biocompatible Ti-based BMGs; (2) develop a complete understanding of the processing-structure-mechanical property relations of Ti-based BMGs and propose new strategies for achieving the room temperature tensile ductility of Ti-based BMGs; (3) address the formability and oxidation resistance of Ti-based BMGs in their supercooled region and improve the thermoplastic formability of Ti-based BMGs; and (4) explore new application areas for Ti-based BMGs.

Acknowledgments: This work was supported by the National Natural Science Foundation of China (Grants No. 51601063, 51575522, and 51271095) and the New Century Talent Supporting Project (Grant No. NCET-11-0185). The authors are grateful to the Analytical and Testing Center, Huazhong University of Science and Technology, for technical assistance. The valuable discussions and support from Yang Shao, Xin Wang, Shaofan Zhao, Shengbao Qiu, Zhen Peng, Guannan Yang, Peng Gui, Zhenyu Song, Jialun Gu, and Zhidog Han are appreciated.

Author Contributions: Pan Gong prepared the manuscript. Pan Gong, Lei Deng, Junsong Jin, and Sibo Wang collected the data. Xinyun Wang and Kefu Yao designed the scope of the paper. All authors discussed the conclusions and reviewed the manuscript.

Conflicts of Interest: The authors declare no conflict of interest.

References

1. Klement, W.K.; Willens, R.H.; Duwez, P. Non-crystalline structure in solidified gold-silicon alloys. *Nature* **1960**, *187*, 869–870. [CrossRef]
2. Chen, H.S. Thermodynamic considerations on formation and stability of metallic glasses. *Acta Metall.* **1974**, *22*, 1505–1511. [CrossRef]
3. Inoue, A.; Nishiyama, N.; Matsuda, T. Preparation of bulk glassy $Pd_{40}Ni_{10}Cu_{30}P_{20}$ alloy of 40 mm in diameter by water quenching. *Mater. Trans. JIM* **1996**, *37*, 181–184. [CrossRef]
4. Nishiyama, N.; Inoue, A. Flux treated Pd–Cu–Ni–P amorphous alloy having low critical cooling rate. *Mater. Trans. JIM* **1997**, *38*, 464–472. [CrossRef]
5. Yokoyama, Y.; Mund, E.; Inoue, A.; Schultz, L. Production of Zr55Cu30Ni5Al10 glassy alloy rod of 30 mm in diameter by a cap-cast technique. *Mater. Trans.* **2007**, *48*, 3190–3192. [CrossRef]
6. Inoue, A.; Nakamura, T.; Sugita, T.; Zhang, T.; Masumoto, T. Bulky La–Al-TM (TM = Transition Metal) amorphous alloys with high tensile strength produced by a high-pressure die casting method. *Mater. Trans.* **1993**, *34*, 351–358. [CrossRef]
7. Inoue, A.; Nakamura, T.; Nishiyama, N.; Masumoto, T. Mg–Cu–Y bulk amorphous alloys with high tensile strength produced by a high-pressure die casting method. *Mater. Trans.* **1992**, *33*, 937–945. [CrossRef]
8. Nishiyama, N.; Takenaka, K.; Miura, H.; Saidoh, N.; Zeng, Y.Q.; Inoue, A. The world's biggest glassy alloy ever made. *Intermetallics* **2012**, *30*, 19–24. [CrossRef]
9. Peker, A.; Johnson, W.L. A highly processable metallic glass: $Zr_{41.2}Ti_{13.8}Cu_{12.5}Ni_{10}Be_{22.5}$. *Appl. Phys. Lett.* **1993**, *63*, 2342–2344. [CrossRef]
10. He, Y.; Schwarz, R.B.; Archuleta, J.I. Bulk glass formation in the Pd–Ni–P system. *Appl. Phys. Lett.* **1996**, *69*, 1861–1863. [CrossRef]
11. Sun, Y.J.; Qu, D.D.; Huang, Y.J.; Liss, K.D.; Wei, X.S.; Xing, D.W.; Shen, J. Zr–Cu–Ni–Al bulk metallic glasses with superior glass-forming ability. *Acta Mater.* **2009**, *57*, 1290–1299. [CrossRef]
12. Zhang, Q.S.; Zhang, W.; Inoue, A. Ni-free Zr–Fe–Al–Cu bulk metallic glasses with high glass-forming ability. *Scr. Mater.* **2009**, *61*, 241–244. [CrossRef]
13. Hua, N.B.; Pang, S.J.; Li, Y.; Wang, J.F.; Li, R.; Georgarakis, K.; Yavari, A.R.; Vaughan, G.; Zhang, T. Ni- and Cu-free Zr-Al-Co-Ag bulk metallic glasses with superior glass-forming ability. *J. Mater. Res.* **2011**, *26*, 539–546. [CrossRef]
14. Huang, B.; Bai, H.Y.; Wang, W.H. Unique properties of CuZrAl bulk metallic glasses induced by microalloying. *J. Appl. Phys.* **2011**, *110*, 123522. [CrossRef]
15. Jia, P.; Guo, H.; Li, Y.; Xu, J.; Ma, E. A new Cu–Hf–Al ternary bulk metallic glass with high glass-forming ability and ductility. *Scr. Mater.* **2006**, *54*, 2165–2168. [CrossRef]

16. Wang, Q.; Dong, C.; Qiang, J.; Wang, Y. Cluster line criterion and Cu–Zr–Al bulk metallic glass formation. *Mater. Sci. Eng. A* **2007**, *449–451*, 18–23. [CrossRef]
17. Zheng, Q.; Ma, H.; Ma, E.; Xu, J. Mg–Cu–(Y, Nd) pseudo-ternary bulk metallic glasses: The effects oof Nd on glass-forming ability and plasticity. *Scr. Mater.* **2006**, *55*, 541–544. [CrossRef]
18. Park, E.S.; Kang, H.G.; Kin, W.T.; Kim, D.H. Effect of Ag addition on the glass-forming ability of Mg–Cu–Y metallic glass alloys. *J. Non-Cryst. Solids* **2001**, *279*, 154–160. [CrossRef]
19. Pang, S.J.; Zhang, T.; Asami, K.; Inoue, A. Synthesis of Fe-Cr-Mo-C-B-P bulk metallic glasses with high corrosion resistance. *Acta Mater.* **2002**, *50*, 489–497. [CrossRef]
20. Li, Q.; Li, J.; Gong, P.; Yao, K.; Gao, J.; Li, H. Formation of bulk magnetic ternary $Fe_{80}P_{13}C_7$ glassy alloy. *Intermetallics* **2012**, *26*, 62–65. [CrossRef]
21. Na, J.H.; Demetriou, M.D.; Floyd, M.; Hoff, A.; Garrett, G.R.; Johnson, W.L. Compositional landscape for glass formation in metal alloys. *PNAS* **2014**, *111*, 9031–9036. [CrossRef] [PubMed]
22. Zeng, Y.; Nishiyama, N.; Inoue, A. Formation of a Ni–based glassy alloy in centimeter scale. *Mater. Trans.* **2007**, *48*, 1355–1358.
23. Wang, J.; Li, R.; Xiao, R.; Xu, T. Compressibility and hardness of Co-based bulk metallic glass: A combined experimental and density functional theory study. *Appl. Phys. Lett.* **2011**, *99*, 151911. [CrossRef]
24. Man, Q.; Sun, H.; Dong, Y.; Shen, B.; Kimura, H.; Makino, A.; Inoue, A. Enhancement of glass-forming ability of CoFeBSiNb bulk glassy alloys with excellent soft-magnetic properties and superhigh strength. *Intermetallics* **2010**, *18*, 1876–1879. [CrossRef]
25. Liang, L.; Hui, X.; Zhang, C.M.; Chen, G.L. An Er-based bulk metallic glass with high thermal stability and excellent magnetocaloric properties. *Intermetallics* **2008**, *16*, 198–201. [CrossRef]
26. Zhang, T.; Li, R.; Pang, S. Effect of similar elements on improving glass-forming ability of La-Ce-based alloys. *J. Alloy. Compd.* **2009**, *483*, 60–63. [CrossRef]
27. Zhang, T.; Inour, A. Bulk glassy alloys with low liquidus temperature in Pt-Cu-P system. *Mater. Trans.* **2003**, *44*, 1143–1146. [CrossRef]
28. Zhang, W.; Guo, H.; Chen, M.W.; Saotome, Y.; Qin, C.L.; Inoue, A. New Au-based bulk glassy alloys with ultralow glass transition temperature. *Scr. Mater.* **2009**, *61*, 744–747. [CrossRef]
29. Jiang, J.Z.; Hofmann, D.; Jarvis, D.J.; Fecht, H.J. Low-density high-strength bulk metallic glasses and their composites: A review. *Adv. Eng. Mater.* **2014**, *17*, 761–780. [CrossRef]
30. Wang, W.H.; Dong, C.; Shek, C.H. Bulk metallic glasses. *Mater. Sci. Eng. R.* **2004**, *44*, 45–89. [CrossRef]
31. Tanner, L.E.; Ray, R. Physical properties of $Ti_{50}Be_{40}Zr_{10}$ glass. *Scr. Mater.* **1977**, *11*, 783–789. [CrossRef]
32. Holloway, K.; Sinclair, R. Amoprhous Ti–Si alloy formed by interdiffusion of amorphous Si and crystalline Ti multilayers. *J. Appl. Phys.* **1987**, *61*, 1359–1364. [CrossRef]
33. Sharma, S.K.; Macht, M.P.; Naundorf, V. Impurity-difussion investigations in amorphous $Ti_{60}Ni_{40}$. *Phys. Rev. B* **1994**, *49*, 6655. [CrossRef]
34. Tanner, L.E.; Ray, R. Metallic glass formation and properties in Zr and Ti alloyed with Be-I the binary Zr–Be and Ti–Be systems. *Acta Metall.* **1979**, *27*, 1727–1747. [CrossRef]
35. Inoue, A.; Kimura, H.M.; Masumoto, T.; Suryanarayana, C.; Hoshi, A. Superconductivity of ductile Ti–Nb–Si amorphous alloys. *J. Appl. Phys.* **1980**, *51*, 5475–5482. [CrossRef]
36. Lu, B.; Li, Y.; Xu, J. Optimal glass-forming composition and its correlation with eutectic reaction in the Ti–Ni–Al ternary system. *J. Alloy. Compd.* **2009**, *467*, 261–267. [CrossRef]
37. Amiya, K.; Nishiyama, N.; Inoue, A.; Masumoto, T. Mechanical strength and thermal stability of Ti-based amorphous alloys with large glass—forming ability. *Mater. Sci. Eng. A* **1994**, *179*, 692–696. [CrossRef]
38. Peker, A.; Johnson, W.L. Beryllium bearing amorphous metallic alloys formed by low cooling rate. U.S. Patent No. 5288344 A 2nd, February 1994.
39. Zhang, T.; Inoue, A. Thermal and mechanical properties of Ti–Ni–Cu–Sn amorphous alloys with a wide supercooled liquid region before crystallization. *Mater. Trans. JIM* **1998**, *39*, 1001–1006. [CrossRef]
40. Wu, X.F.; Suo, Z.Y.; Si, Y.; Meng, L.K.; Qiu, K.Q. Bulk metallic glass formation in a ternary Ti–Cu–Ni alloy system. *J. Alloy. Compd.* **2008**, *452*, 268–272. [CrossRef]
41. Wang, Y.L.; Xu, J. Ti (Zr)–Cu–Ni bulk metallic glasses with optimal glass-forming ability and their compressive properties. *Metall. Mater. Trans. A* **2008**, *39*, 2990–2997. [CrossRef]

42. Wiest, A.; Duan, G.; Demetriou, D.; Wiest, L.A.; Peck, A.; Kaltenboeck, G.; Wiest, B.; Johnson, W.L. Zr-Ti-based Be-bearing glasses optimized for high thermal stability and thermoplastic formability. *Acta Mater.* **2008**, *56*, 2625–2630. [CrossRef]
43. Nagahama, D.; Ohkubo, T.; Hono, K. Crystallization of $Ti_{36}Zr_{24}Be_{40}$ metallic glass. *Scr. Mater.* **2003**, *49*, 729–734. [CrossRef]
44. He, G.; Eckert, J.; Hagiwara, M. Glass-forming ability and crystallization behavior of Ti–Cu–Ni–Sn-M (M = Zr, Mo, and Ta) metallic glass. *J. Appl. Phys.* **2004**, *95*, 1816–1821. [CrossRef]
45. Xie, K.F.; Yao, K.F.; Huang, T.Y. A Ti-based bulk glassy alloy with high strength and good glass-forming ability. *Intermetallics* **2010**, *18*, 1837–1841. [CrossRef]
46. Zhu, S.L.; Wang, X.M.; Qin, F.X.; Yoshimura, M.; Inoue, A. New TiZrCuPd quaternary bulk glassy alloys with potential of biomedical applications. *Mater. Trans.* **2007**, *48*, 2445–2448. [CrossRef]
47. Zhu, S.L.; Wang, X.M.; Inoue, A. Glass-forming ability and mechanical properties of Ti-based bulk glassy alloys with large diameters of up to 1 cm. *Intermetallics* **2008**, *16*, 1031–1035. [CrossRef]
48. Qin, F.; Wang, X.; Zhu, S.; Kawashima, A.; Asami, K.; Inoue, A. Fabrication and corrosion property of novel Ti-based bulk glassy alloys without Ni. *Mater. Trans.* **2007**, *48*, 515–518. [CrossRef]
49. Zhu, S.; Wang, X.; Qin, F.; Inoue, A. Glass-forming ability and thermal stability of Ti–Zr–Cu–Pd–Si bulk glassy alloys for biomedical applications. *Mater. Trans.* **2007**, *48*, 163–166. [CrossRef]
50. Qin, F.X.; Wang, X.M.; Xie, G.Q.; Inoue, A. Distinct plastic strain of Ni-free Ti–Zr–Cu–Pd–Nb bulk metallic glasses with potential for biomedical applications. *Intermetallics* **2008**, *16*, 1026–1030. [CrossRef]
51. Kim, Y.C.; Park, J.M.; Lee, J.K.; Bae, D.H.; Kim, W.T.; Kim, D.H. Amorphous and icosahedral phases in Ti–Zr–Cu–Ni–Be alloys. *Mater. Sci. Eng. A* **2004**, *375–377*, 749–753. [CrossRef]
52. Guo, F.; Wang, H.J.; Poon, S.J.; Shiflet, G.J. Ductile titanium-based glassy alloy ingots. *Appl. Phys. Lett.* **2005**, *86*, 091907. [CrossRef]
53. Park, J.M.; Wang, G.; Pauly, S.; Mattern, N.; Kim, D.H.; Eckert, J. Ductile Ti-based bulk metallic glasses with high specific strength. *Metall. Mater. Trans. A* **2011**, *42*, 1456–1462. [CrossRef]
54. Huang, Y.J.; Shen, J.; Sun, J.F.; Yu, X.B. A new Ti–Zr–Hf–Cu–Ni–Si–Sn bulk amorphous alloy with high glass-forming ability. *J. Alloy. Compd.* **2007**, *427*, 171–175. [CrossRef]
55. Liu, Y.; Pang, S.; Li, H.; Hu, Q.; Chen, B.; Zhang, T. Formation and properties of Ti-based Ti–Zr–Cu–Fe–Sn–Si bulk metallic glasses with different (Ti + Zr)/Cu ratios for biomedical application. *Intermetallics* **2016**, *72*, 36–43. [CrossRef]
56. Pang, S.; Liu, Y.; Li, H.; Sun, L.; Li, Y.; Zhang, T. New Ti-based Ti–Cu–Zr–Fe–Sn–Si–Ag bulk metallic glass for biomedical applications. *J. Alloy. Compd.* **2015**, *625*, 323–327. [CrossRef]
57. Liu, Y.; Wang, G.; Li, H.; Pang, S.; Chen, K.; Zhang, T. Ti–Cu–Zr–Fe–Sn–Si–Sc bulk metallic glasses with good mechanical properties for biomedical applications. *J. Alloy. Compd.* **2016**, *679*, 341–349. [CrossRef]
58. Lou, H.B.; Wang, X.D.; Xu, F.; Ding, S.Q.; Cao, Q.P.; Hono, K.; Jiang, J.Z. 73 mm-diameter bulk metallic glass rod by copper mold casting. *Appl. Phys. Lett.* **2011**, *99*, 051910. [CrossRef]
59. Shen, J.; Chen, Q.J.; Sun, J.F.; Fan, H.B.; Wang, G. Exceptionally high glass-forming ability of an FeCoCrMoCBY alloy. *Appl. Phys. Lett.* **2005**, *86*, 151907. [CrossRef]
60. Zheng, Q.; Xu, J.; Ma, E. High glass-forming ability correlated with fragility of Mg–Cu(Ag)-Gd alloys. *J. Appl. Phys.* **2007**, *102*, 113519. [CrossRef]
61. Zeng, Y.; Nishiyama, N.; Yamamoto, T.; Inoue, A. Ni–rich bulk metallic glasses with high glass-forming ability and good metallic properties. *Mater. Trans.* **2009**, *50*, 2441–2445. [CrossRef]
62. Zhou, B.W.; Zhang, W.; Zhang, X.G.; Kimura, H.; Makino, A.; Inoue, A. Foormation and thermal stability of Cu-based metallic glasses with high glass-forming ability. *Metall Mater. Trans. A* **2012**, *43*, 2592–2597. [CrossRef]
63. Zhang, T.; Yang, Q.; Ji, Y.F.; Li, R.; Pang, S.J.; Wang, J.F.; Xu, T. Centimeter-scale-diameter Co-based bulk metallic glasses with fracture strength exceeding 5000 MPa. *Chin. Sci. Bull.* **2011**, *56*, 3972–3977. [CrossRef]
64. Schroers, J.; Johnson, W.L. Highly processable bulk metallic glass-forming alloys in the Pt–Co–Ni–Cu-P system. *Appl. Phys. Lett.* **2004**, *84*, 3666–3668. [CrossRef]
65. Guo, H.; Zhang, W.; Qin, C.; Qiang, J.; Chen, M.; Inoue, A. Glass-forming ability and properties of new AU-based glassy alloys with low Au concentrations. *Mater. Trans.* **2009**, *50*, 1290–1293. [CrossRef]
66. Laws, K.J.; Shamlaye, K.F.; Ferry, M. Synthesis of Ag-based bulk metallic glass in the Ag-Mg-Ca-[Cu] alloy system. *J. Alloy. Compd.* **2012**, *513*, 10–13. [CrossRef]

67. Senkov, O.N.; Miracle, D.B.; Keppens, V.; Liaw, P.K. Development and characterization of low-density Ca-based bulk metallic glasses: an overview. *Metall. Mater. Trans. A* **2008**, *39*, 1888–1900. [CrossRef]
68. Wu, N.C.; Zuo, L.; Wang, J.Q.; Ma, E. Designing aluminum-rich bulk metallic glasses via electronic-structure-guided microalloying. *Acta Mater.* **2016**, *108*, 143–151. [CrossRef]
69. Xu, T.; Pang, S.; Li, H.; Zhang, T. Corrosion resistant Cr-based bulk metallic glasses with high strength and hardness. *J. Non-Cryst. Solids* **2015**, *410*, 20–25. [CrossRef]
70. Jiang, Q.K.; Zhang, G.Q.; Yang, L.; Wang, X.D.; Saksl, K.; Franz, H.; Wunderlich, R.; Fecht, H.; Jiang, J.Z. La-based bulk metallic glasses with critical diameter up to 30 mm. *Acta Mater.* **2007**, *55*, 4409–4418. [CrossRef]
71. Zhou, Y.; Zhao, Y.; Qu, B.Y.; Wang, L.; Zhou, R.L.; Wu, Y.C.; Zhang, B. Remarkable effect of Ce base element purity upon glass-forming ability in Ce-Ga–Cu bulk metallic glasses. *Intermetallics* **2015**, *56*, 56–62. [CrossRef]
72. Tang, M.Q.; Zhang, H.F.; Zhu, Z.W.; Fu, H.M.; Wang, A.M.; Li, H.; Hu, Z.Q. TiZr-base bulk metallic glass with over 50 mm in diameter. *J. Mater. Sci. Tech.* **2010**, *26*, 481–486. [CrossRef]
73. Zhang, L.; Tang, M.; Zhu, Z.W.; Fu, H.M.; Zhang, H.W.; Wang, A.M.; Li, H.; Zhang, H.F.; Hu, Z.Q. Compressive plastic metallic glass with exceptional glass-forming ability in the Ti–Zr–Cu–Fe–Be alloy system. *J. Alloy. Compd.* **2015**, *638*, 349–355. [CrossRef]
74. Inoue, A.; Zhang, T.; Masumoto, T. Glass-forming ability of alloys. *J. Non-Cryst. Solids* **1993**, *156–158*, 473–480. [CrossRef]
75. Turnbull, D. Under what conditions can a glass be formed? *Contemp. Phys.* **1969**, *10*, 473–488. [CrossRef]
76. Lu, Z.P.; Liu, C.T. A new glass-forming ability criterion for bulk metallic glasses. *Acta Mater.* **2002**, *50*, 3501–3512. [CrossRef]
77. Guo, S.; Lu, Z.P.; Liu, C.T. Identify the best glass-forming ability criterion. *Intermetallics* **2010**, *18*, 883–888. [CrossRef]
78. Zhang, G.H.; Chou, K.C. A criterion for evaluating glass-forming ability of alloys. *J. Appl. Phys.* **2009**, *106*, 094902. [CrossRef]
79. Duan, G.; Wiest, A.; Lind, M.L.; Kahl, A.; Johnson, W.L. Lightweight Ti-based bulk metallic glasses excluding late transition metals. *Scr. Mater.* **2008**, *58*, 465–468. [CrossRef]
80. Hao, G.J.; Lin, J.P.; Zhang, Y.; Chen, G.L.; Lu, Z.P. Ti–Zr–Be ternary bulk metallic glasses correlated with binary eutectic clusters. *Mater. Sci. Eng. A* **2010**, *527*, 6248–6250. [CrossRef]
81. Zhang, Y.; Zhang, W.G.; Lin, J.P.; Hao, G.J.; Chen, G.L.; Liaw, P.K. Glass-forming ability and competitive crystalline phases for lightweight Ti–Be-based alloys. *Metall. Mater. Trans. A* **2010**, *41*, 1670–1676. [CrossRef]
82. Men, H.; Pang, S.; Inoue, A.; Zhang, T. New Ti-based bulk metallic glasses with significant plasticity. *Mater. Trans.* **2005**, *46*, 2218–2220. [CrossRef]
83. Wang, Z.R.; Dong, D.D.; Qiang, J.B.; Wang, Q.; Wang, Y.M.; Dong, C. Ti-based glassy alloys in Ti–Cu–Ni–Sn system. *Sci. China Phys. Mech. Astron.* **2013**, *56*, 1419–1422. [CrossRef]
84. Kim, Y.C.; Kim, W.T.; Kim, D.H. A development of Ti-based buulk metallic glass. *Mater. Sci. Eng. A* **2004**, *375–377*, 127–135. [CrossRef]
85. Liu, Y.; Xu, J. Optimized compositions of Ti-(Cu, Ni)–Sn alloy for metallic glass formation and their correlation with eutectic reaction. *Acta Metall. Sin.* **2008**, *44*, 1424–1430.
86. Zhu, S.L.; Wang, X.M.; Qin, F.X.; Inoue, A. A new Ti-based bulk glassy alloy with potential for biomedical application. *Mater. Sci. Eng. A* **2007**, *459*, 233–237. [CrossRef]
87. Gong, P.; Yao, K.F.; Shao, Y. Effects of Fe addition on glass-forming ability and mechanical properties of Ti–Zr–Be bulk metallic glass. *J. Alloy Compd.* **2012**, *536*, 26–29. [CrossRef]
88. Gong, P.; Yao, K.; Wang, X.; Shao, Y. A new centimeter-sized Ti-based quaternary bulk metallic glass with good mechanical properties. *Adv. Eng. Mater.* **2013**, *15*, 691–696. [CrossRef]
89. Gong, P.; Wang, X.; Shao, Y.; Chen, N.; Yao, K.F. Ti–Zr–Be–Fe quaternary bulk metallic glasses designed by Fe alloying. *Sci. China Phys. Mech. Astron.* **2013**, *56*, 2090–2097. [CrossRef]
90. Gong, P.; Yao, K.F.; Shao, Y. Lightweight Ti–Zr–Be–Al bulk metallic glasses with improved glass-forming ability and compressive plasticity. *J. Non-Cryst. Solids* **2012**, *358*, 2620–2625. [CrossRef]
91. Zhao, S.F.; Shao, Y.; Gong, P.; Yao, K.F. A centimeter-sized quaternary Ti–Zr–Be-Ag bulk metallic glass. *Adv. Mater. Sci. Eng.* **2014**, *6453*, 163–168. [CrossRef]
92. Zhao, S.F.; Chen, N.; Gong, P.; Yao, K.F. New centimeter-sized quaternary Ti–Zr–Be–Cu bulk metallic glasses with large glass-forming ability. *J. Alloy. Compd.* **2015**, *647*, 533–538. [CrossRef]

93. Zhao, S.F.; Gong, P.; Li, J.F.; Chen, N.; Yao, K.F. Quaternary Ti–Zr–Be–Ni bulk metallic glasses with large glass-forming ability. *Mater. Des.* **2015**, *85*, 564–573. [CrossRef]
94. Zhao, S.; Chen, N.; Gong, P.; Yao, K. Centimeter-sized quaternary Ti-based bulk metallic glasses with high Ti content of 50 atom %. *Adv. Eng. Mater.* **2016**, *18*, 231–235. [CrossRef]
95. Huang, Y.J.; Shen, J.; Sun, J.F. Formation, thermal stability and mechanical properties of $Ti_{42.5}Zr_{7.5}Cu_{40}Ni_5Sn_5$ bulk metallic glass. *Sci. China Phys. Mech. Astron.* **2008**, *51*, 372–378. [CrossRef]
96. Zhang, T.; Inoue, A. Preparation of Ti–Cu–Ni–Si–B amorphous alloys with a large supercooled liquid region. *Mater. Trans. JIM* **1999**, *40*, 301–306. [CrossRef]
97. Khalifa, H.E.; Vecchio, K.S. Thermal stability and crystallization phenomena of low cost Ti-based bulk metallic glass. *J. Non-Cryst. Solids* **2011**, *357*, 3393–3398. [CrossRef]
98. Li, P.; Wang, G.; Ding, D.; Shen, J. Glass forming ability, thermodynamics and mechanical properties of novel Ti–Cu–Ni–Zr–Hf bulk metallic glasses. *Mater. Des.* **2014**, *53*, 145–151. [CrossRef]
99. Ma, C.; Soejima, H.; Ishihara, S.; Amiya, K.; Nishiyama, N.; Inoue, A. New Ti-based bulk glassy alloys with high glass-forming ability and superior mechanical properties. *Mater. Trans.* **2004**, *45*, 3223–3227. [CrossRef]
100. Zhang, L.; Zhu, Z.W.; Wang, A.M.; Li, H.; Fu, H.M.; Zhang, H.W.; Zhang, H.F.; Hu, Z.Q. A $Ti_{36.2}Zr_{30.3}Cu_{8.3}Fe_4Be_{21.2}$ bulk metallic glass with exceptional glass-forming ability and remarkable compressive plasticity. *J. Alloy. Compd.* **2013**, *562*, 205–210. [CrossRef]
101. Gong, P.; Wang, X.; Shao, Y.; Chen, N.; Liu, X.; Yao, K.F. A Ti–Zr–Be–Fe–Cu bulk metallic glass with superior glass-forming ability and high specific strength. *Intermetallics* **2013**, *43*, 177–181. [CrossRef]
102. Gong, P.; Yao, K.F.; Wang, X.; Shao, Y. Centimeter-sized Ti-based bulk metallic glass with high specific strength. *Prog. Nat. Sci. Mater. Int.* **2012**, *22*, 401–406. [CrossRef]
103. Zhang, T.; Inoue, A. Ti-based amorphous alloys with a large supercooled liquid region. *Mater. Sci. Eng. A* **2001**, *304–306*, 771–774. [CrossRef]
104. Yin, E.; Zhang, M.; Pang, S.; Zhao, X.; Zhang, T. Formation of Ti–Zr–Cu–Ni–Sn–Si bulk metallic glasses with good plasticity. *J. Alloy. Compd.* **2010**, *504*, S10–S13. [CrossRef]
105. Kim, Y.C.; Bae, D.H.; Kim, W.T.; Kim, D.H. Glass forming ability and crystallization behavior of Ti-based amorphous alloys with high specific strength. *J. Non-Cryst. Solids* **2003**, *325*, 242–250. [CrossRef]
106. Hao, G.J.; Zhang, Y.; Lin, J.P.; Wang, Y.L.; Lin, Z.; Chen, G.L. Bulk metallic glass formation of Ti-based alloys from low purity elements. *Mater. Lett.* **2006**, *60*, 1256–1260. [CrossRef]
107. Xia, M.; Zheng, H.; Liu, J.; Ma, C.; Li, J. Thermal stability and glass-forming ability of new Ti-based bulk metallic glasses. *J. Non-Cryst. Solids* **2005**, *351*, 3747–3751. [CrossRef]
108. Ma, C.; Ishihara, S.; Soejima, H.; Nishiyama, N.; Inoue, A. Formatiion of new Ti-based metallic glassy alloys. *Mater. Trans.* **2004**, *45*, 1802–1806. [CrossRef]
109. Xia, M.X.; Ma, C.L.; Zheng, H.X.; Li, J.G. Preparation and crystallization of $Ti_{53}Cu_{27}Ni_{12}Zr_3Al_7Si_3B_1$ bulk metallic glass with wide supercooled liquid region. *Mater. Sci. Eng. A* **2005**, *390*, 372–375. [CrossRef]
110. Wang, T.; Wu, Y.D.; Si, J.J.; Cai, Y.H.; Chen, X.H.; Hui, X.D. Novel Ti-based bulk metallic glasses with superior plastic yielding strength and corrosion resistance. *Mater. Sci. Eng. A* **2015**, *642*, 297–303. [CrossRef]
111. Murty, B.S.; Ranganathan, S.; Rao, M.M. Solid state amorphization in binary Ti–Ni, Ti–Cu and ternary Ti–Ni–Cu system by mechanical alloying. *Mater. Sci. Eng. A* **1992**, *149*, 231–240. [CrossRef]
112. Nash, P.; Choo, H.; Schwarz, R.B. Thermodynamic calculation of phase equilibria in the Ti–Co and Ni–Sn systems. *J. Mater. Sci.* **1998**, *33*, 4929–4936. [CrossRef]
113. Zhang, S.; Sumiyama, K.; Nakamura, Y. Nonequilibrium crystalline and amorphous Ti–Pd alloys produced by vapor quenching. *Mater. Trans. JIM* **1989**, *30*, 733–740. [CrossRef]
114. Inoue, A. Stabilization of metallic supercooled liquid and bulk amorphous alloys. *Acta Mater.* **2000**, *48*, 279–306. [CrossRef]
115. Takeuchi, A.; Inoue, A. Classification of bulk metallic glasses by atomic size difference, heat of mixing and period of constituent elements and its application to characterization of the main alloying element. *Mater. Trans.* **2005**, *46*, 2817–2829. [CrossRef]
116. Li, R.; Pang, S.; Ma, C.; Zhang, T. Influence of similar atom substitution on glass formation in (La-Ce)–Al–Co bulk metallic glasses. *Acta Mater.* **2007**, *55*, 3719–3726. [CrossRef]
117. Wang, H.; Park, E.S.; Oak, J.J.; Setyawan, A.D.; Zhu, S.L.; Wada, T.; Takeuchi, A.; Kato, H. Effect of cobalt microalloying on the glass-forming ability of Ti–Cu–Pd–Zr metallic glass. *J. Non-Cryst. Solids* **2013**, *379*, 155–160. [CrossRef]

118. Xu, F.; Lou, H.B.; Wang, X.D.; Ding, S.Q.; Cao, Q.P.; Jiang, J.Z. Glass forming ability and crystallization of Zr-Cu-Ag-Al-Be bulk metallic glasses. *J. Alloy. Compd.* **2011**, *509*, 9034–9037. [CrossRef]
119. Xiao, X.; Fang, S.; Wang, G.; Hua, Q.; Dong, Y. Influence of beryllium on the thermal stability and glass-forming ability of Zr–Al–Ni–Cu bulk amorphous alloys. *J. Alloy. Compd.* **2004**, *376*, 145–148. [CrossRef]
120. Inoue, A.; Zhang, T.; Kurosaka, K.; Zhang, W. High-strength Cu-based bulk glassy alloys in Cu–Zr-Ti–Be system. *Mater. Trans.* **2001**, *42*, 1800–1804. [CrossRef]
121. Park, J.M.; Chang, H.J.; Han, K.H.; Kim, W.T.; Kim, D.H. Enhancement of plasticity in Ti-rich Ti–Zr–Be–Cu–Ni bulk metallic glasses. *Scr. Mater.* **2005**, *53*, 1–6. [CrossRef]
122. Wang, W.H. Roles of minor additions in formation and properties of bulk metallic glasses. *Prog. Mater. Sci.* **2007**, *52*, 540–596. [CrossRef]
123. Lu, Z.P.; Liu, C.T. Role of minor alloying additions in formation of bulk metallic glasses: A review. *J. Mater. Sci.* **2004**, *39*, 3965–3974. [CrossRef]
124. Chen, N.; Martin, L.; Luzguine-Luzgin, D.V.; Inoue, A. Role of alloying additions in glass formation and properties of bulk metallic glasses. *Materials* **2010**, *3*, 5320–5339. [CrossRef]
125. Cao, D.; Wu, Y.; Wang, H.; Liu, X.J.; Lu, Z.P. Effects of nitrogen on the glass formation and mechanical properties of a Ti-based metallic glass. *Acta Metall. Sin. Eng. Lett.* **2016**, *29*, 173–180. [CrossRef]
126. Wang, T.; Wu, Y.D.; Si, J.J.; Hui, X.D. Effects of Zr and Si on the glass-forming ability and compressive properties of Ti–Cu–Co–Sn alloys. *Metall. Mater. Trans. A* **2015**, *46*, 2381–2389. [CrossRef]
127. Hao, G.; Ren, F.; Zhang, Y.; Lin, J. Role of yttrium in glass formation in Ti-based bulk metallic glasses. *Rare Met.* **2009**, *28*, 68–71. [CrossRef]
128. Mei, J.N.; Li, J.S.; Kou, H.C.; Fu, H.Z.; Zhou, L. Effects of Nb on the formation of icosahedral quasicrystalline phase in Ti-rich Ti–Zr–Ni–Cu–Be glassy forming alloys. *J. Non-Cryst. Solids* **2008**, *354*, 3332–3335. [CrossRef]
129. Li, L.; Liu, R.; Zhao, J.; Cai, H.; Yang, Z. Effects of Nb addition on glass-forming ability, thermal stability and mechanical properties of Ti-based bulk metallic glasses. *Rare Met. Matter. Eng.* **2014**, *43*, 1835–1838. [CrossRef]
130. Xie, K.F.; Yao, K.F.; Huang, T.Y. Preparation of $(Ti_{0.45}Cu_{0.378}Zr_{0.10}Ni_{0.072})_{100-x}Sn_x$ bulk metallic glasses. *J. Alloy. Compd.* **2010**, *504*, S22–S26. [CrossRef]
131. Liu, C.T.; Chissholm, M.F.; Miller, M.K. Oxygen impurity and microalloying effect in a Zr-based bulk metallic glass alloy. *Intermetallics* **2002**, *10*, 1105–1112. [CrossRef]
132. Kundig, A.A.; Lepori, D.; Perry, A.J.; Rossmann, S.; Blatter, A.; Dommann, A.; Uggowitzer, P.J. Influence of low oxygen contents and alloy refinement on the glass-forming ability of $Zr_{52.5}Cu_{17.9}Ni_{14.6}Al_{10}Ti_5$. *Mater. Trans.* **2002**, *43*, 3206–3210. [CrossRef]
133. Lu, Z.P.; Liu, C.T.; Ported, W.D. Role of yttrium in glass formation of Fe-based bulk metallic glasses. *Appl. Phys. Lett.* **2003**, *83*, 2581–2583. [CrossRef]
134. Yan, M.; Shen, J.; Zhang, T.; Zou, J. Enhanced glass-forming ability of a Zr-based bulk metallic glass with yttrium doping. *J. Non-Cryst. Solids* **2006**, *352*, 3109–3112. [CrossRef]
135. Egami, T.; Waseda, Y. Atomic size effect on the formability of metallic glasses. *J. Non-Cryst. Solids* **1984**, *64*, 113–134. [CrossRef]
136. Senkov, O.N.; Miracle, D.B. Effect of the atomic size distribution on glass-forming abilty of amorphous metallic alloys. *Mater. Res. Bull.* **2001**, *36*, 2183–2198. [CrossRef]
137. Yun, Y.S.; Nam, H.S.; Cha, P.R.; Kim, W.T.; Kim, D.H. Effects of atomic size difference and heat of mixing parameters on the local structure of a model metallic glass system. *Met. Mater. Int.* **2014**, *20*, 105–111. [CrossRef]
138. Louzguine-Luzgin, D.V.; Inoue, A.; Botta, W.J. Reduced electronegativity difference as a factor leading to the formation of Al-based glassy alloys with a large supercooled liquid region of 50 K. *Appl. Phys. Lett.* **2006**, *88*, 011911. [CrossRef]
139. Ma, C.S.; Zhang, J.; Chang, X.C.; Hou, W.L.; Wang, J.Q. Electronegativity difference as a factor for evaluating the thermal stability of Al-rich metallic glasses. *Philos. Mag. Lett.* **2008**, *88*, 917–924. [CrossRef]
140. Jiao, Z.B.; Li, H.X.; Gao, J.E.; Wu, Y.; Lu, Z.P. Effects of alloying elements on glass formation, mechanical and soft-magnetic properties of Fe-based metallic glasses. *Intermetallics* **2011**, *19*, 1502–1508. [CrossRef]
141. Schuh, C.A.; Hufnagel, T.C.; Ramamurty, U. Mechanical behavior of amorphous alloys. *Acta Mater.* **2007**, *55*, 4067–4109. [CrossRef]

142. Trexler, M.M.; Thadhani, N.N. Mechanical properties of bulk metallic glasses. *Porg. Mater. Sci.* **2010**, *55*, 759–839. [CrossRef]
143. Kruzic, J.J. Bulk metallic glasses as structural materials: A review. *Adv. Eng. Mater.* **2016**. [CrossRef]
144. Inoue, A.; Takeuchi, A. Recent progress in bulk glassy alloys. *Mater. Trans.* **2002**, *43*, 1892–1906. [CrossRef]
145. Wang, G.; Fan, H.B.; Huang, Y.J.; Shen, J.; Chen, Z.H. A new TiCuHfSi bulk metallic glass with potential for biomedical applications. *Mater. Des.* **2014**, *54*, 252–255. [CrossRef]
146. Yao, K.F.; Yang, Y.Q.; Chen, N. Mechanical properties of Pd–Cu–Si bulk metallic glass. *Intermetallics* **2007**, *15*, 639–643. [CrossRef]
147. Yang, B.J.; Yao, J.H.; Zhang, J.; Yang, H.W.; Wang, J.Q.; Ma, E. Al-rich bulk metallic glasses with plasticity and ultrahigh specific strength. *Scr. Mater.* **2009**, *61*, 423–426. [CrossRef]
148. Salimon, A.L.; Ashby, M.F.; Brechet, Y. Bulk metallic glasses: What are they good for? *Mater. Sci. Eng. A* **2004**, *375–377*, 385–388. [CrossRef]
149. Poon, S.J.; Zhu, A.; Shiflet, G.J. Poisson's ratio and intrinsic plasticity of metallic glasses. *Appl. Phys. Lett.* **2008**, *92*, 261902. [CrossRef]
150. Wei, Y.; Lei, X.; Huo, L.S.; Wang, W.H.; Greer, A.L. Towards more uniform deformation in metallic glasses: The role of Poisson's ratio. *Mater. Sci. Eng. A* **2013**, *560*, 510–517. [CrossRef]
151. Pan, D.G.; Zhang, H.F.; Wang, A.M.; Wang, Z.G.; Hu, Z.Q. Fracture instability in brittle Mg-based bulk metallic glasses. *J. Alloy. Compd.* **2007**, *438*, 145–149. [CrossRef]
152. Guo, S.F.; Qiu, J.L.; Yu, P.; Xie, S.H.; Chen, W. Fe-based bulk metallic glasses: Brittle or ductile? *Appl. Phys. Lett.* **2014**, *105*, 161901. [CrossRef]
153. Xi, X.K.; Zhao, D.Q.; Pan, M.X.; Wang, W.H.; Wu, Y.; Lewandowski, J.J. Fracture of brittle metallic glasses: Brittleness or plasticity. *Phys. Res. Lett.* **2005**, *94*, 125510. [CrossRef] [PubMed]
154. Hofmann, D.C.; Suh, J.Y.; Wiest, A.; Duan, G.; Lind, M.L.; Demetriou, M.D.; Johnson, W.L. Designing metallic glass matrix composites with high toughness and tensile ductility. *Nature* **2008**, *451*, 1085–1089. [CrossRef] [PubMed]
155. Hofmann, D.C.; Suh, J.Y.; Wiest, A.; Lind, M.L.; Demetriou, M.D.; Johnson, W.L. Development of tough, low-density titanium-based bulk metallic glass matrix composites with tensile ductility. *PNAS* **2008**, *105*, 20136–20140. [CrossRef] [PubMed]
156. Jeon, C.; Lee, H.; Kim, C.P.; Joo, S.H.; Lee, S. Effects of effective dendrite size on tensile deformation behavior in Ti-based dendrite-containing amorphous matrix composites modified form Ti–6Al–4V alloy. *Metall. Mater. Trans. A* **2015**, *46*, 235–250. [CrossRef]
157. Huang, Y.J.; Shen, J.; Sun, J.F. Bulk metallic glasses: Smaller is softer. *Appl. Phys. Lett.* **2007**, *90*, 081919. [CrossRef]
158. Lee, C.J.; Huang, J.C.; Nieh, T.G. Sample size effect and microcompression of $Mg_{65}Cu_{25}Gd_{10}$ metallic glass. *Appl. Phys. Lett.* **2007**, *91*, 161913–162100. [CrossRef]
159. Wu, W.F.; Han, Z.; Li, Y. Size-dependent "malleable-to-brittle" transition in a bulk metallic glass. *Appl. Phys. Lett.* **2008**, *93*, 061908. [CrossRef]
160. Yang, Y.; Liu, C.T. Size effect on stability of shear-band propagation in bulk metallic glasses: An overview. *J. Mater. Sci.* **2012**, *47*, 55–67. [CrossRef]
161. Wu, F.F.; Zhang, Z.F.; Mao, S.X.; Eckert, J. Effect of sample size on ductility of metallic glass. *Philos. Mag. Lett.* **2009**, *89*, 178–184. [CrossRef]
162. Wang, X.Y.; Deng, L.; Tang, N.; Jin, J.S. Size effect on flow behavior of a $Zr_{55}Al_{10}Ni_5Cu_{30}$ bulk metallic glass in supercooled liquid state. *Metall. Mater. Trans. A* **2014**, *45*, 3505–3511. [CrossRef]
163. Yao, D.; Deng, L.; Zhang, M.; Wang, X.; Tang, N.; Li, J. A size-depenedent constitutive model of bulk metallic glasses in the supercooled liquid reion. *Sci. Rep.* **2015**, *5*, 8083. [CrossRef] [PubMed]
164. Jiang, W.H.; Fan, G.J.; Choo, H.; Liaw, P.K. Ductility of a Zr-based bulk-metallic glass with different specimen's geometries. *Mater. Lett.* **2006**, *60*, 3537–3540. [CrossRef]
165. Huang, Y.; Shen, J.; Sun, J.; Zhang, Z. Enhanced strength and plasticity of a Ti-based metallic glass at cryogenic temperatures. *Mater. Sci. Eng. A* **2008**, *498*, 203–207. [CrossRef]
166. Yu, P.; Bai, H.Y. Poisson's ratio and plasticity in CuZrAl bulk metallic glass. *Mater. Sci. Eng. A* **2008**, *485*, 1–4. [CrossRef]
167. Lewandowski, J.J.; Wang, W.H.; Greer, A.L. Intrisic plasticity or brittleness of metallic glass. *Philos. Mag. Lett.* **2005**, *85*, 77–87. [CrossRef]

168. Qiao, J.W.; Jia, H.L.; Liaw, P.K. Metallic glass matrix composites. *Mater. Sci. Eng. R* **2016**, *100*, 1–69. [CrossRef]
169. Schramm, J.P.; Hofmann, D.C.; Demetriou, M.D.; Johnson, W.L. Metallic-glass-matrix composite structure with benchmark mechanical performance. *Appl. Phys. Lett.* **2010**, *97*, 241910. [CrossRef]
170. He, G.; Loser, W.; Eckert, J.; Schultz, J. Enhanced plasticity in a Ti-based bulk metallic glass-forming alloy by in situ formation of a composite microstructure. *J. Mater. Res.* **2002**, *17*, 3015–3018. [CrossRef]
171. Tang, M.; Zhu, Z.; Fu, H.; Wang, A.; Li, H.; Zhang, H.; Ma, G.; Zhang, H.; Hu, Z. Ti-based amorphous composites with quantitatively controlled in-situ formation of dendrites. *Acta Metall. Sin.* **2012**, *48*, 861–866. [CrossRef]
172. Cui, J.; Li, J.S.; Wang, J.; Kou, H.C. Microstructure evolution of a Ti-based bulk metallic glass composite during deformation. *J. Mater. Eng. Perform.* **2015**, *24*, 748–753. [CrossRef]
173. Zhang, Z.Y.; Wu, Y.; Zhou, J.; Wang, H.; Liu, X.J.; Lu, Z.P. Strong work-hardening behavior in a Ti-based bulk metallic glass composite. *Scr. Mater.* **2013**, *69*, 73–76. [CrossRef]
174. Yang, S.; Li, D.; Wang, X.S.; Guo, J.W.; Zhang, S.F.; He, L. Mechanical behavior and wear performance of a Ti-based bulk metallic glass composite containing dendritic and intermetallic phases. *Mater. Sci. Eng. A* **2016**, *672*, 135–142. [CrossRef]
175. Park, J.M.; Jayaraj, J.; Kim, D.H.; Mattern, N.; Wang, G.; Eckert, J. Tailoring of in situ Ti-based bulk glassy matrix composites with high mechanical performance. *Intermetallics* **2010**, *18*, 1908–1911. [CrossRef]
176. Khalifa, H.E.; Vecchio, K.S. High strength $(Ti_{58}Ni_{28}Cu_8Si_4Sn_2)_{100-x}Mo_x$ nanoeutectic matrix-β-Ti dendrite, BMG-derived composites with enhanced plasticity and corrosion resistance. *Adv. Eng. Mater.* **2009**, *11*, 885–891. [CrossRef]
177. Ma, D.Q.; Jiao, W.T.; Zhang, Y.F.; Wang, B.A.; Li, J.; Zhang, X.Y.; Ma, M.Z.; Liu, R.P. Strong work-hardening behavior induced by the solid solution strengthening of dendrites in TiZr-based bulk metallic glass matrix composites. *J. Alloy. Compd.* **2015**, *624*, 9–16. [CrossRef]
178. Zhang, J.; Qiao, J.; Zhang, Y. Synthesis of plastic lightweight Ti-based metallic-glass-matrix composites by Bridgman solidification. *Acta Metall. Sin.* **2011**, *47*, 236–240.
179. Wang, Y.S.; Hao, G.J.; Zhang, Y.; Lin, J.P.; Song, L.; Qiao, J.W. The role of the interface in a Ti-based metallic glass matrix composite with in situ dendrite reinforcement. *Surf. Interface Anal.* **2014**, *46*, 293–296. [CrossRef]
180. Wang, D.J.; Huang, Y.J.; Wu, L.Z.; Shen, J. Mechanical behaviors of diamond reinforced Ti-based bulk metallic glassy composites prepared by spark plasma sintering. *J. Alloy. Compd.* **2013**, *560*, 841–846. [CrossRef]
181. Qiao, J.W. In-situ dendrite/metallic glass matrix composites: A review. *J. Mater. Sci. Tech.* **2013**, *29*, 685–701. [CrossRef]
182. Jun, H.J.; Lee, K.S.; Kim, C.P.; Chang, Y.W. Ductility enhancement of a Ti-based bulk metallic glass through annealing treatment below the glass transition temperature. *Intermetallics* **2012**, *20*, 47–54. [CrossRef]
183. Cao, Q.P.; Liu, J.W.; Yang, K.J.; Xu, F.; Yao, Z.Q.; Minkow, A.; Fecht, H.J.; Ivanisenko, J.; Chen, L.Y.; Wang, X.D.; et al. Effect of pre-existing shear bands on the tensile mechanical properties of a bulk metallic glass. *Acta Mater.* **2010**, *58*, 1276–1292. [CrossRef]
184. Qiu, S.B.; Yao, K.F.; Gong, P. Work toughening effect of $Zr_{41}Ti_{14}Cu_{12.5}Ni_{10}Be_{22.5}$ bulk metallic glass. *Chin. Sci. Bull.* **2011**, *56*, 3942–3947. [CrossRef]
185. Huang, Y.; Sun, Y.; Shen, J. Tuning the mechanical performance of a Ti-based bulk metallic glass by pre-deformation. *Intermetallics* **2010**, *18*, 2044–2050. [CrossRef]
186. Park, J.M.; Kim, D.H.; Eckert, J. Internal state modulation-mediate plasticity enhancement in monolithic Ti-based bulk metallic glass. *Intermetallics* **2012**, *29*, 70–74. [CrossRef]
187. Nieh, T.G.; Yang, Y.; Lu, J.; Liu, C.T. Effect of surface modification on shear banding and plasticity in metallic glasses: An overview. *Prog. Nat. Sci. Mater. Int.* **2012**, *22*, 355–363. [CrossRef]
188. Zhang, Y.; Wang, W.H.; Greer, A.L. Making metallic glasses plastic by control of residual stress. *Nat. Mater.* **2006**, *5*, 857–860. [CrossRef] [PubMed]
189. Chen, W.; Chan, K.C.; Yu, P.; Wang, G. Encapsulated Zr-based bulk metallic glass with large plasticity. *Mater. Sci. Eng. A* **2011**, *528*, 2988–2994. [CrossRef]
190. Qiu, S.B.; Yao, K.F. Novel application of the electrodeposition on bulk metallic glasses. *Appl. Surf. Sci.* **2008**, *255*, 3454–3458. [CrossRef]
191. Fan, J.; Chen, A.; Wang, J.; Shen, J.; Lu, J. Improved plasticity and fracture toughness in metallic glasses via surface crystallization. *Intermetallics* **2011**, *19*, 1420–1427. [CrossRef]
192. Madge, S.V. Toughness of bulk metallic glasses. *Metals* **2015**, *5*, 1279–1305. [CrossRef]

193. Wang, G.; Zhao, D.Q.; Bai, H.Y.; Pan, M.X.; Xia, A.L.; Han, B.S.; Xi, X.K.; Wu, Y.; Wang, W.H. Nanoscale periodic morphologies on the fracture surface of brittle metallic glasses. *Phys. Rev. Lett.* **2007**, *98*, 235501. [CrossRef] [PubMed]
194. Lewandowski, J.J.; Gu, X.J.; Nouri, A.S.; Poon, S.J.; Shiflet, G.J. Tough Fe-based bulk metallic glasses. *Appl. Phys. Lett.* **2008**, *92*, 091918. [CrossRef]
195. Demetriou, M.D.; Launey, M.E.; Garrett, G.; Schramm, J.P.; Hofmann, D.C.; Johnson, W.L.; Ritchie, R.O. A damage-tolerant glass. *Nat. Mater.* **2011**, *10*, 123–128. [CrossRef] [PubMed]
196. Gu, X.J.; Poon, S.J.; Shiflet, G.J.; Lewandowski, J.J. Compressive plasticity and toughness of a Ti-based bulk metallic glass. *Acta Mater.* **2010**, *58*, 1708–1720. [CrossRef]
197. Chen, W.; Ketkaew, J.; Liu, Z.; Mota, R.M.O.; O'Brien, K.; Silva, C.S.D.; Schroers, J. Does the fracture toughness of bulk metallic glasses scatter? *Scr. Mater.* **2015**, *107*, 1–4. [CrossRef]
198. Yamaura, S.; Zhu, S.; Abe, K.; Xie, G. Ultrasonic fatigue of $Ti_{40}Zr_{10}Cu_{34}Pd_{14}Sn_2$ glassy alloy. *Open J. Met.* **2014**, *4*, 56–64. [CrossRef]
199. Fujita, K.; Hashimoto, H.; Zhang, W.; Nishiyama, N.; Ma, C.; Kimura, H.; Inoue, A. Ultrahigh fatigue strength in Ti-based bulk metallic glasses. *Rev. Adv. Mater. Sci.* **2008**, *18*, 137–139.
200. Wang, G.Y.; Liaw, P.K.; Peker, A.; Yang, B.; Benson, M.L.; Yuan, W.; Peter, W.H.; Huang, L.; Freels, M.; Buchanan, R.A.; et al. Fatigue behavior of Zr-Ti–Ni–Cu–Be bulk-metallic glasses. *Intermetallics* **2005**, *13*, 429–435. [CrossRef]
201. Fujita, K.; Zhang, W.; Shen, B.; Amiya, K.; Ma, C.; Nishiyama, N. Fatigue properties in high strength bulk metallic glasses. *Intermetallics* **2012**, *30*, 12–18. [CrossRef]
202. Peter, M.; Gysler, A.; Lutjering, G. Influence of texture on fatigue properties of Ti–6Al–4V. *Metall. Mater. Trans. A* **1984**, *15*, 1597–1605. [CrossRef]
203. Schroers, J.; Nguyen, T.; O'Keeffe, S.; Desai, A. Thermoplastic forming of bulk metallic glass-applications for MEMS and microstructure fabrication. *Mater. Sci. Eng. A* **2007**, *449–451*, 898–902. [CrossRef]
204. Schroers, J. Processing of bulk metallic glass. *Adv. Mater.* **2010**, *22*, 1566–1597. [CrossRef] [PubMed]
205. Li, N.; Chen, W.; Liu, L. Thermoplastic micro-forming of bulk metallic glasses: A review. *JOM* **2016**, *68*, 1246–1261. [CrossRef]
206. Schroers, J. On the formability of bulk metallic glass in its supercooled liquid state. *Acta Mater.* **2008**, *56*, 471–478. [CrossRef]
207. Fan, G.J.; Fecht, H.J.; Lavernia, E.J. Viscous flow of the $Pd_{43}Ni_{10}Cu_{27}P_{20}$ metallic glass-forming liquid. *Appl. Phys. Lett.* **2004**, *84*, 487–489. [CrossRef]
208. Legg, B.A.; Schroers, J.; Busch, R. Thermodynamics, kinetics, and crystallization of $Pt_{57.3}Cu_{14.6}Ni_{5.3}P_{22.8}$ bulk metallic glass. *Acta Mater.* **2007**, *55*, 1109–1116. [CrossRef]
209. Schroers, J.; Lohwongwatana, B.; Johnson, W.L.; Peker, A. Gold based bulk metallic glasses. *Appl. Phys. Lett.* **2005**, *87*, 061912. [CrossRef]
210. Mukherjee, S.; Schroers, J.; Zhou, Z.; Johnson, W.L.; Rhim, W.K. Viscosity and specific volume of bulk metallic glass-forming alloys and their correlation with glass-forming ability. *Acta Mater.* **2004**, *52*, 3689–3695. [CrossRef]
211. Waniuk, T.A.; Schroers, J.; Johnson, W.L. Critical cooling rate and thermal stability of Zr-Ti–Cu–Ni–Be alloys. *Appl. Phys. Lett.* **2001**, *778*, 1213–1215. [CrossRef]
212. Busch, R.; Liu, W.; Johnson, W.L. Thermodynamics and kinetics of the $Mg_{65}Cu_{25}Y_{20}$ bulk metallic glass-forming liquid. *J. Appl. Phys.* **1998**, *83*, 4134–4141. [CrossRef]
213. Park, S.H.; Lim, K.R.; Na, M.Y.; Kim, Y.C.; Kim, W.T.; Kim, D.H. Oxidation behavior of Ti–Cu binary metallic glass. *Corros. Sci.* **2015**, *99*, 304–312. [CrossRef]
214. Park, S.H.; Lim, K.R.; Na, M.Y.; Kim, Y.C.; Kim, W.T.; Kim, D.H. Effect of minor addition of Zr on the oxidation behavior of Ti–Cu metallic glass. *Corros. Sci.* **2016**, *22*, 229–235.
215. Zhang, M.; Yao, D.; Wang, X.; Deng, L. Air oxidation of a $Zr_{55}Cu_{30}Al_{10}Ni_5$ bulk metallic glass at its super cooled liquid state. *Corros. Sci.* **2014**, *82*, 410–419. [CrossRef]
216. Li, N.; Xu, X.; Zheng, Z.; Liu, L. Enhanced formability of a Zr-based bulk metallic glass in a supercooled liquid state by vibrational loading. *Acta Mater.* **2014**, *65*, 400–411. [CrossRef]
217. Liu, Z.; Schroers, J. General nanomoulding with bulk metallic glasses. *Nanotechnology* **2015**, *26*, 143501. [CrossRef] [PubMed]

218. Morrison, M.L.; Buchanan, R.A.; Peker, A.; Liaw, P.K.; Horton, J.A. Electrochemical behavior of a Ti-based bulk metallic glass. *J. Non-Cryst. Solids* **2007**, *353*, 2115–2124. [CrossRef]
219. Fornell, J.; Pellicer, E.; Steenberge, N.V.; Gonzalez, S.; Surinach, S.; Baro, M.D.; Sort, J. Improved plasticity and corrosion behavior in Ti–Zr–Cu–Pd metallic glass with minor additions of Nb: An alloy composition intended for biomedical applications. *Mater. Sci. Eng. A* **2013**, *559*, 159–164. [CrossRef]
220. Qin, F.; Wang, X.; Kawashima, A.; Zhu, S.; Kimura, H.; Inoue, A. Corrosion behavior of Ti-based metallic glasses. *Mater. Trans.* **2006**, *47*, 1934–1937. [CrossRef]
221. Qin, F.; Yoshimura, M.; Wang, X.; Zhu, S.; Kawashima, A.; Asami, K.; Inoue, A. Corrosion behavior of a Ti-based bulk metallic glass and its crystalline alloys. *Mater. Trans.* **2007**, *48*, 1855–1858. [CrossRef]
222. Li, H.F.; Zheng, Y.F. Recent advances in bulk metallic glasses for biomedical applications. *Acta Biomater.* **2016**, *36*, 1–20. [CrossRef] [PubMed]
223. Calin, M.; Gebert, A.; Ghinea, A.C.; Gostin, P.F.; Abdi, S.; Mickel, C.; Eckert, J. Designing biocompatible Ti-based metallic glasses for implant applications. *Mater. Sci. Eng. C* **2013**, *33*, 875–883. [CrossRef] [PubMed]
224. Niinomi, M. Mechanical biocompatibilities of titanium alloys for biomedical applications. *J. Mech. Behav. Biomed.* **2008**, *1*, 30–42. [CrossRef] [PubMed]
225. Wang, W.H. Correaltions between elastic moduli and properties in bulk metallic glasses. *J. Appl. Phys.* **2006**, *99*, 093506. [CrossRef]
226. Huang, C.H.; Lai, J.J.; Wei, T.Y.; Chen, Y.H.; Wang, X.; Kuan, S.Y.; Huang, J.C. Improvement of bio-corrosion resistance for $Ti_{42}Zr_{40}Si_{15}Ta_3$ metallic glasses in simulated body fluid by annealing within supercooled liquid region. *Mater. Sci. Eng. C* **2015**, *52*, 144–150. [CrossRef] [PubMed]
227. Oak, J.J.; Inoue, A. Attempt to develop Ti-based amorphous alloys for biomaterials. *Mater. Sci. Eng. A* **2007**, *449–451*, 220–224. [CrossRef]
228. Huang, H.H.; Sun, Y.S.; Wu, C.P.; Liu, C.F.; Liaw, P.K.; Wu, K. Corrosion resistance and biocompatibility of Ni-free Zr-based bulk metallic glass for biomedical applications. *Intermetallics* **2012**, *30*, 139–143. [CrossRef]
229. Wang, Y.B.; Li, H.F.; Cheng, Y.; Zheng, Y.F.; Ruan, L.Q. In vitro and in vivo studies on Ti-based bulk metallic glass as potential dental implant material. *Mater. Sci. Eng. C* **2013**, *33*, 3489–3497. [CrossRef] [PubMed]
230. Kukubun, R.; Wang, W.; Zhu, S.; Xie, G.; Ichinose, S.; Itoh, S.; Takakuda, K. In vivo evaluation of a Ti-based bulk metallic glass alloy bar. *Bio-med. Mater. Eng.* **2015**, *26*, 9–17. [CrossRef] [PubMed]
231. Nishiyama, N.; Amiya, K.; Inoue, A. Novel applications of bulk metallic glass for industrial products. *J. Non-Cryst. Solids* **2007**, *353*, 3615–3621. [CrossRef]
232. Inoue, A.; Takeuchi, A. Recent development and application products of bulk glassy alloys. *Acta Mater.* **2011**, *59*, 2243–2267. [CrossRef]
233. Axinte, E.M.; Chirileanu, M.P.I. Recent progress in the industrialization of metallic glass. *Recent Pat. Mater. Sci.* **2012**, *5*, 213–221. [CrossRef]
234. Wang, X.; Tang, N.; Zheng, Z.; Tang, Y.; Li, J.; Liu, L. A Maxwell-pulse constitutive model of $Zr_{55}Cu_{30}Al_{10}Ni_5$ metallic glass in supercooled liquid region. *J. Alloy. Compd.* **2011**, *509*, 2518–2522. [CrossRef]
235. Li, S.; Horikawa, S.; Park, M.; Chai, Y.; Vodyanoy, V.J.; Chi, B.A. Amorphous metallic glass biosensors. *Intermetallics* **2012**, *30*, 80–85. [CrossRef]
236. Nishiyama, N.; Amiya, A.; Inoue, A. Recent progress of bulk metallic glasses for strain-sensing devices. *Mater. Sci. Eng. A* **2007**, *449–451*, 79–83. [CrossRef]
237. Ashby, M.F.; Greer, A.L. Metallic glasses as structural materials. *Scr. Mater.* **2006**, *54*, 321–326. [CrossRef]
238. Khun, N.W.; Yu, H.; Chong, Z.Z.; Tian, P.; Tian, Y.; Tor, S.B.; Liu, E. Mechanical and tribological properties of Zr-based bulk metallic glass for sports applications. *Mater. Des.* **2016**, *92*, 667–673. [CrossRef]
239. Wang, X.; Shao, Y.; Gong, P.; Yao, K.F. The effect of simulated thermal cycling on thermal and mechanical stability of a Ti-based bulk metallic glass. *J. Alloy. Compd.* **2013**, *575*, 449–454.
240. Wang, X.; Gong, P.; Shao, Y.; Yao, K.F. Chemical composition dependence of atomic oxygen erosion resistance in Ti-based bulk metallic glasses. Unpublished work, 2016.